FACULTY OF SCIENCE
UNIVERSITY OF COPENHAGEN

Master's thesis

Magnetic Triplet Excitations in Graphene

Logi Arnarson

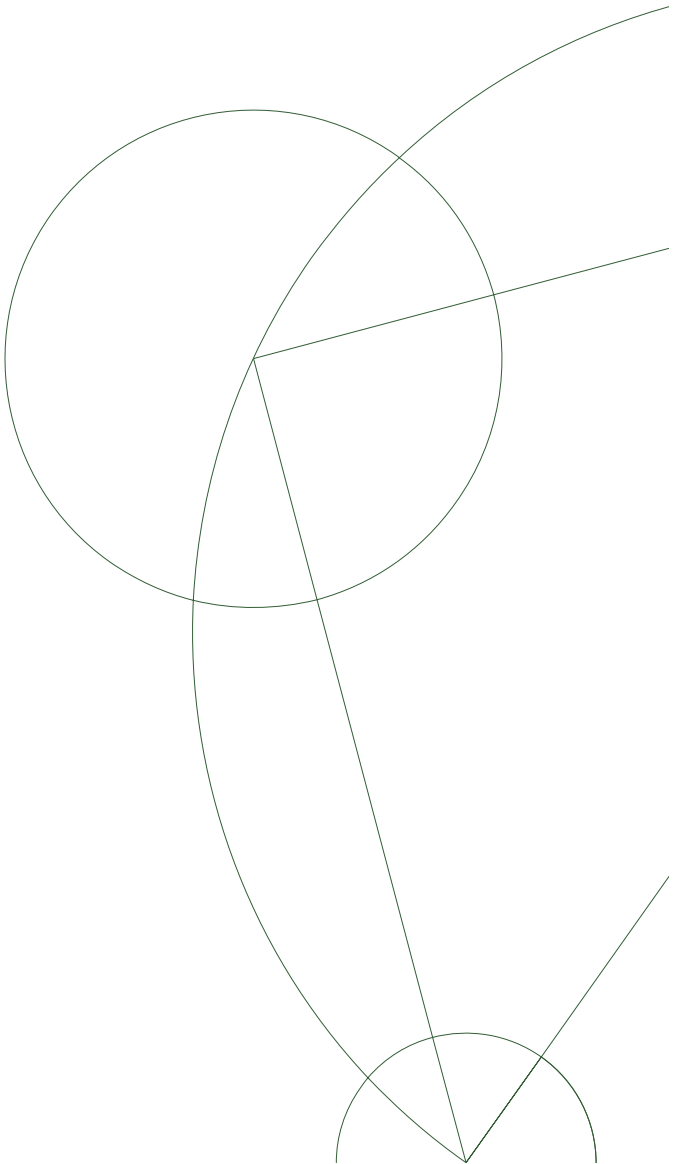

Academic Advisor:
Per Hedegård
Niels Bohr Institute
University of Copenhagen

Submitted: August 1, 2012

Fyrir Ömmu og Afa...

Abstract

When doping graphene an unique window appears in the electron–hole excitation spectrum. Including the Coulomb interaction through the Hubbard Hamiltonian results in bound state formation in graphene. The bound states we analyze represent triplet excitations, i.e. magnons, with spin 1. When increasing the strength of the Coulomb interaction, electron–hole pairs are dragged down into the window. This is a property of the triplet excitations since the interaction term is negative, indicating attraction, in that context. We analyzed further the dispersion relation for $U \simeq 11\,\mathrm{eV}$ and at last we investigated the appearance of magnons in real space.

Résumé

Når man doper grafen opstår der et unikt vindue i elektron–hul eksitation spektret. Inklusionen af Coulomb vekselvirkningen gennem Hubbard Hamiltonianen resulterer i dannelsen af bundne tilstande i grafen. De bundne tilstande der analyseres representerer triplet eksitationer, i.e. magnoner, med spin 1. Forøges styrken af Coulomb vekselvirkningen, bliver elektron–hul parrerne trukket ned i vinduet. Det er en egenskab af triplet eksistationerne eftersom vekselvirknings ledet er negativt, hvilket indikerer tiltrækning i denne kontekst. Yderligere analyserede vi dispersion relationen for $U \simeq 11\,\mathrm{eV}$ og til sidst undersøgte vi hvordan magnoner opstår i det reele rum.

Preface

A new era in condensed matter physics began when in 2004, Andre Geim and Konstantin Novoselov, published a paper on electric field effect in atomically thin carbon films [1]. Living in times where the silicon based technology is approaching its limits and soon can not be engineered to faster, thinner and lighter electronics, graphene is a possible solution. Despite enormous growth in graphene research since its discovery, 8 years ago, there is still a lot to learn. The properties of materials are largely dependent on how the electrons within the material behave and interact. In the theory of interaction between electrons in graphene a lot of bricks are still missing. In this thesis we take these interaction into account and analyze their consequences in hope to fill into one of the holes found in the theory of graphene.

I would like to thank my supervisor, Professor Per Hedegård, for teaching me physics from his inspiring point of view. I would also like to thank my colleagues from the office who have always been very helpful and entertaining. At last big thanks to Nanna, Svanhvít and Örn, Elmar and Sigrún, Telma Lísa, Hugi, Sölvi and Nökkvi for being very supportive all the time.

Contents

Chapter 1

Introduction and motivation

In the first chapter we will define the problem we are going to attack in this thesis and give an introduction to the fundamental properties of graphene. We will also motivate the research by taking examples from other materials where including the Coulomb interaction was a success.

1.1 The problem

We want to analyze the Coulomb interaction in graphene, the wonder material first observed and isolated in 2004 which has the potential to effect our everyday life drastically in the upcoming decades. The first thing one reads about graphene is its conical dispersion relation and from there many of its amazing properties are derived. All this happens in the absence of taking any interaction between the electrons in the material into account. In organic molecules containing carbon hexagons of same structure as those found in graphene the Coulomb interaction are vital. The Hubbard model often used in condensed matter physics reveals this antithesis. In molecules the Hubbard Hamiltonian, $\mathcal{H}_{hub} = \mathcal{H}_{hop} + \mathcal{H}_{int}$, is often approximated as

$$\mathcal{H}_{hub} \sim \mathcal{H}_{int},$$

whereas in graphene

$$\mathcal{H}_{hub} \sim \mathcal{H}_{hop}.$$

This simply can not expose the complete story about graphene. We can consider graphene as being a giant organic molecule and the fact that the strong correlations present in molecules are not inherited at all in this extreme limit is puzzling. We will in the upcoming chapters include the electron–electron interaction and see how that changes and affects the single particle picture described by the hopping term in the Hubbard model. We will analyze two different situations where this process has lead us to discover new interesting physics in the past. In both cases the inclusion of the Coulomb interaction has generated formation of bound states. Bound states of nucleons, atoms, molecules and solids

allow the world and all life in it to be the way it is. These states are formed when the interaction energy between two objects is less than the total energy of each object separately. Bound states are consequently stable and have infinite lifetime unless energy is spent. Finding these states in materials is of immense importance and in our case including the Coulomb interaction of electrons in graphene could help us identifying one of these.

1.2 Outline of thesis

For overview purposes we would like to outline what is about to happen in the rest of the thesis. In this first and rather long chapter we will give an introduction to graphene and define what it is and how it is formed. We will also motivate our research both by analyzing how the Coulomb interaction affects the simplest of all molecules, the H_2 molecule and also see how including interaction effects results in the formation of bound states in two specific situations. In Chapter 2 we will go in details with the Hubbard model in graphene, derive its famous dispersion relation and at last formulate the interaction term in k-space. That turns out to be non-trivial due to graphene's crystal structure. In Chapter 3 we will analyze what the interaction part of the Hamiltonian really stands for and utilize in the subspace of interest. In Chapter 4 we solve the Schrödinger equation for the given problem with numerical methods and in the last chapter we will discuss the results by going back to real space.

1.3 The hydrogen molecule

In this section we would like to look at a simple example to show how the Coulomb interaction are vital in the world of molecules. A molecule is defined as a discrete neutral species resulting from covalent bond formation between two or more atoms [2]. Now let's look at how the chemical bond between to hydrogen atoms is formed to make the H_2 molecule. What is meant by the term "chemical bond" is that, by allowing the wave functions of the delocalized electrons in play, to spread over two or more atoms the energy of the whole system is decreased and a bound state is formed. In the case of two hydrogen atoms each containing one proton and one electron the total energy of the system is decreased by formation of molecular orbitals. These can either be spatially symmetric (bonding) or antisymmetric (antibonding). In H_2 the bonding orbital is lower in energy which is due to the antibonding orbital has greater curvature and therefore larger kinetic energy as can be seen in Fig. 1.1. The bonding orbitals for the system we have in mind, the H_2 molecule are

$$\phi_b(r) = \frac{1}{\sqrt{2}} \left(\phi_1(r) + \phi_2(r) \right), \tag{1.1}$$

where ϕ_1 and ϕ_2 are the two s-orbitals of the hydrogen atoms. Each electron carries a spin so therefore different configurations of the system are possible.

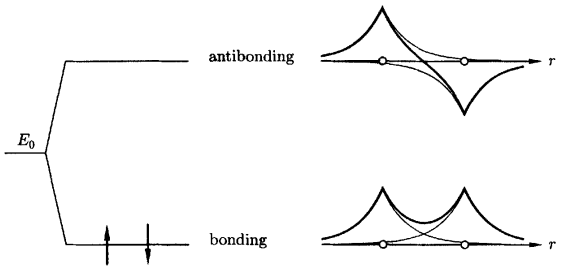

Figure 1.1: On the figure we see the molecular orbitals for a diatomic molecule, f.ex. H_2. Their energy is also indicated to the left, showing that it costs more energy to construct an antibonding (antisymmetric) orbital than a bonding (symmetric) orbital.[3]

The Slater determinant gives us the wave function of this many-body (two-body) fermionic system that has to respect Pauli's exclusion principle,

$$\Phi(r_1, r_2) = \frac{1}{\sqrt{2}} \begin{vmatrix} \phi_{b\uparrow}(r_1) & \phi_{b\uparrow}(r_2) \\ \phi_{b\downarrow}(r_1) & \phi_{b\downarrow}(r_2) \end{vmatrix}. \tag{1.2}$$

In second quantization language an electron in a bonding orbital with spin σ is created by $c^\dagger_{b\sigma} = {}^1\!/\!\sqrt{2}(c^\dagger_{1\sigma} + c^\dagger_{2\sigma})$. Eq. (1.2) therefore becomes

$$\Phi = \frac{1}{\sqrt{2}} \left(c^\dagger_{1\uparrow} c^\dagger_{2\downarrow} - c^\dagger_{1\downarrow} c^\dagger_{2\uparrow} + c^\dagger_{1\uparrow} c^\dagger_{1\downarrow} + c^\dagger_{2\uparrow} c^\dagger_{2\downarrow} \right) |0\rangle, \tag{1.3}$$

where each operator creates an electron in an s-orbital either at hydrogen atom 1 or 2 with spin either $\uparrow$ or $\downarrow$. What Eq. (1.3) implies is that there is 50% probability of finding the two electrons residing on the same atom which is unrealistic since the repulsive Coulomb interaction between electron must prevent this to happen. To make our model more realistic we apply the Hubbard Hamiltonian which assumes well localized electrons that have the ability to tunnel from one atom to another but have to pay a penalty of U if they find themselves on the same atom (we will discuss the Hubbard Hamiltonian in more details in Section 2.1). There are six possible configurations having two electrons and two protons, namely the two electrons are both at the same atom and therefore have to have opposite spin due to their fermionic properties, the two electrons are at different atoms with opposite spin and at last the two electrons are at different atoms with same spin. The basis therefore consists of these six two electron states

$$\mathcal{B} = \left\{ c^\dagger_{1\uparrow} c^\dagger_{1\downarrow} |0\rangle, c^\dagger_{2\uparrow} c^\dagger_{2\downarrow} |0\rangle, c^\dagger_{1\uparrow} c^\dagger_{2\downarrow} |0\rangle, c^\dagger_{2\uparrow} c^\dagger_{1\downarrow} |0\rangle, c^\dagger_{1\uparrow} c^\dagger_{2\uparrow} |0\rangle, c^\dagger_{1\downarrow} c^\dagger_{2\downarrow} |0\rangle \right\}. \tag{1.4}$$

The Hamiltonian in this basis takes the form

$$\mathcal{H} = \begin{pmatrix} U & 0 & -t & -t & 0 & 0 \\ 0 & U & -t & -t & 0 & 0 \\ -t & -t & 0 & 0 & 0 & 0 \\ -t & -t & 0 & 0 & 0 & 0 \\ 0 & 0 & 0 & 0 & 0 & 0 \\ 0 & 0 & 0 & 0 & 0 & 0 \end{pmatrix} \tag{1.5}$$

where we have defined the energy of the s-orbitals to be zero and t the hopping energy from one atom to another $-t = \langle\phi_1|\mathcal{H}|\phi_2\rangle = \langle\phi_2|\mathcal{H}|\phi_1\rangle$ which is nothing but the energy overlap of the two electron wave functions. The Hamiltonian in Eq. (1.5) can be made simpler by transforming to a new basis which are eigenstates of the parity operator P and spin operator S_z. The new basis is then

$$\begin{aligned} \mathcal{B}' = \Big\{ & \frac{1}{\sqrt{2}}(c^\dagger_{1\uparrow}c^\dagger_{1\downarrow} - c^\dagger_{2\downarrow}c^\dagger_{2\uparrow})|0\rangle, \frac{1}{\sqrt{2}}(c^\dagger_{1\uparrow}c^\dagger_{1\downarrow} + c^\dagger_{2\downarrow}c^\dagger_{2\uparrow})|0\rangle, \\ & \frac{1}{\sqrt{2}}(c^\dagger_{1\uparrow}c^\dagger_{2\downarrow} - c^\dagger_{1\downarrow}c^\dagger_{2\uparrow})|0\rangle, \frac{1}{\sqrt{2}}(c^\dagger_{1\uparrow}c^\dagger_{2\downarrow} + c^\dagger_{1\downarrow}c^\dagger_{2\uparrow})|0\rangle, \\ & c^\dagger_{1\uparrow}c^\dagger_{2\uparrow}|0\rangle, c^\dagger_{1\downarrow}c^\dagger_{2\downarrow}|0\rangle \Big\}. \end{aligned} \tag{1.6}$$

We are allowed to use these eigenstates instead since our Hamiltonian commutes with both P and S_z i.e. $[\mathcal{H}, P] = [\mathcal{H}, S_z] = 0$. In this new basis the Hamiltonian becomes

$$\mathcal{H} = \begin{pmatrix} U & 0 & -2t & 0 & 0 & 0 \\ 0 & U & 0 & 0 & 0 & 0 \\ -2t & 0 & 0 & 0 & 0 & 0 \\ 0 & 0 & 0 & 0 & 0 & 0 \\ 0 & 0 & 0 & 0 & 0 & 0 \\ 0 & 0 & 0 & 0 & 0 & 0 \end{pmatrix}. \tag{1.7}$$

We find the eigenvalues and eigenvectors of the Hamiltonian in Eq. (1.7) which are

i) Ground state:

$$E_0 = U - \sqrt{U + 16t^2}, \tag{1.8a}$$

$$|E_0\rangle = \left(\frac{\sqrt{1+\delta}}{2}(c^\dagger_{1\uparrow}c^\dagger_{2\downarrow} - c^\dagger_{1\downarrow}c^\dagger_{2\uparrow})\right) + \frac{\sqrt{1-\delta}}{2}(c^\dagger_{1\uparrow}c^\dagger_{1\downarrow} - c^\dagger_{2\downarrow}c^\dagger_{2\uparrow})|0\rangle, \tag{1.8b}$$

where $\delta = \dfrac{U}{\sqrt{U^2 + 16t^2}}$.

ii) First excited states:

$$E_1 = 0, \tag{1.9a}$$

$$|E_1\rangle = \begin{cases} c^\dagger_{1\uparrow}c^\dagger_{2\uparrow}|0\rangle \\ \frac{1}{\sqrt{2}}(c^\dagger_{1\uparrow}c^\dagger_{2\downarrow} + c^\dagger_{1\downarrow}c^\dagger_{2\uparrow})|0\rangle \\ c^\dagger_{1\downarrow}c^\dagger_{2\downarrow}|0\rangle \end{cases} . \tag{1.9b}$$

The first excited state turns out to be three-folded i.e. three states share the same energy.

iii) Second excited state:

$$E_2 = U, \tag{1.10a}$$

$$|E_2\rangle = \frac{1}{\sqrt{2}}(c^\dagger_{1\uparrow}c^\dagger_{1\downarrow} + c^\dagger_{2\downarrow}c^\dagger_{2\uparrow})|0\rangle. \tag{1.10b}$$

iv) Third excited state:

$$E_3 = U + \sqrt{U + 16t^2}, \tag{1.11a}$$

$$|E_3\rangle = \left(\frac{\sqrt{1-\delta}}{2}(c^\dagger_{1\uparrow}c^\dagger_{2\downarrow} - c^\dagger_{1\downarrow}c^\dagger_{2\uparrow})\right) - \frac{\sqrt{1+\delta}}{2}(c^\dagger_{1\uparrow}c^\dagger_{1\downarrow} - c^\dagger_{2\downarrow}c^\dagger_{2\uparrow})|0\rangle, \tag{1.11b}$$

where agin $\delta = \dfrac{U}{\sqrt{U^2 + 16t^2}}$.

What we see from this is that the ground state Eq. (1.8) is a spin singlet whereas the first excited state Eq. (1.9) is a spin triplet. In the case of strong Coulomb interaction where $U >> t$ the ground state energy is approximated by

$$E_0 \approx -\frac{8t^2}{U}, \tag{1.12}$$

with eigenstate

$$|E_0\rangle \approx \frac{1}{\sqrt{2}}(c^\dagger_{1\uparrow}c^\dagger_{2\downarrow} - c^\dagger_{1\downarrow}c^\dagger_{2\uparrow})|0\rangle. \tag{1.13}$$

This result tells us that the electrons are well localized one on each atom and recovers the Heitler–London prediction that the total energy of the system is minimized by the generation of molecular orbitals of delocalized electron wave functions. In the opposite limit $U << t$ we recover what we got in Eq. (1.3) where the electrons behave as they were independent which in the case of molecules they certainly are not.[4]

Even though in this section we only described the most simplest molecule of them all the result is unambiguous and holds also for larger molecules. The interaction between electrons in molecules can not be neglected in the process of describing the world correctly.

1.4 Graphene

In this section we describe the fundamental properties of graphene both in real space and reciprocal space. We also touch briefly upon the history and future of graphene and see how the discovery of this highly rated material was kind of an serendipity.

1.4.1 Fundamental properties of graphene

Carbon is number six in the periodic table meaning it has six protons and six electrons in its neutral form. Four of these six electrons are valence electrons i.e. electrons that participate in making chemical bonds with other atoms as they are weakly bound to the core compared to the $1s$ electrons. They fill the $2s$ orbital and two of three $2p$ orbitals in the x and y directions. When carbon forms a crystal one of the $2s$ electrons gains energy from the nearest neighbouring nuclei and excites to the empty $2p_z$ orbital all in all lowering the total energy of crystal making it a stable material. Due to low energy difference between the $2s$ and $2p_{x,y}$ energy levels compared to the energy stored in the chemical bonds the wave function of these electrons can mix internally making the carbon–carbon bonding stronger. This process is called hybridization and the electron configuration of both freestanding- and crystalized carbon are shown in Figs. 1.2(a) and (b).

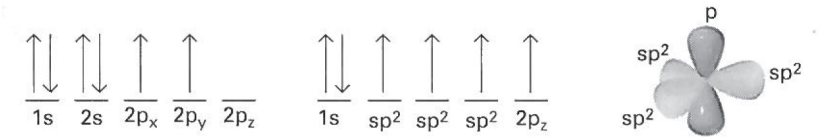

(a) Electron configuration of freestanding carbon.

(b) Electron configuration of hybridized carbon.

(c) The electron orbitals of hybridized carbon.

Figure 1.2: In the figures we can see the electron configuration of both isolated carbon, carbon present in a crystal forming graphene and the electronic orbitals in graphene.[5]

Graphene is defined as a planar allotrope of carbon where all the carbon atoms form in–planar bonds due to hybridization called sp^2-bonds or σ-bonds illustrated in Fig. 1.2(c). They are the strongest type of covalent bonds and are responsible for graphene's great strength. The unpaired electron in the $2p_z$ orbital perpendicular to the carbon plane makes a covalent bond called a π-bond which is much weaker than the σ-bond. It can therefore be considered as delocalized and is responsible for the electronic properties of graphene.[6] [5]

Graphene is a single atomic layer of carbon atoms and can therefore be considered as effectively two-dimensional. No material can be made thinner. In Fig. 1.3 we can see the graphene plane along with other materials also only consisting of carbon atoms. Graphene is the mother material of these three allotropes, the zero-dimensional buckyball formed by wrapping of graphene, one-dimensional carbon nanotube formed by folding graphene and three-dimensional graphite formed by stacking graphene.[7]

Now we would like to describe the crystal structure of graphene and define both

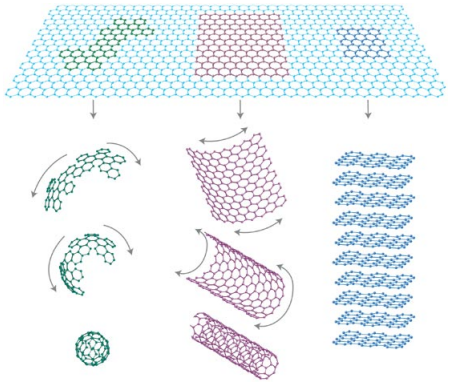

Figure 1.3: Graphene along with the other pure carbon materials that all can be derived from the 2D plain by wrapping (0D buckyball), folding (1D carbon nanotube) or stacking (3D graphite).[7]

its real and reciprocal lattice. A central concept in describing crystalline solids is the Bravais lattice which is defined as an periodic array of discrete points with an arrangement and orientation that looks exactly the same regardless from which point is viewed. The points can represent single atoms, groups of atoms, molecules or some other unit to be considered. In our case they represent an unit, forming a hexagonal lattice, consisting of two carbon atoms called A and B, see Fig. 1.4(a). The hexagonal lattice is though not one of the five unique 2D Bravais lattices since it is not the same to view for example along the x–axis from points A and B. It can though be mapped onto a Bravais lattice by considering the basis which says how many atoms are linked to each Bravais lattice point, consisting of two nonequivalent atoms, namely A and B. Any Bravais lattice point can be captured by the position vector in real space

$$\mathbf{R} = n_1\mathbf{a}_1 + n_2\mathbf{a}_2, \tag{1.14}$$

where n_1 and n_2 are integers and $\mathbf{a}_1$ and $\mathbf{a}_2$ are primitive lattice vectors that span the hexagonal lattice defined as

$$\mathbf{a}_1 = \left(\frac{\sqrt{3}a}{2}, \frac{a}{2}\right), \tag{1.15a}$$

$$\mathbf{a}_2 = \left(\frac{\sqrt{3}a}{2}, -\frac{a}{2}\right), \tag{1.15b}$$

where $a = \sqrt{3}a_{c-c}$ and $a_{c-c} = 1.42\,\text{Å}$ is the nearest neighbour carbon–carbon distance.

The smallest unit needed to fill space without overlapping itself or leaving gaps in between, is called the primitive unit cell. The choice of a primitive unit cell is

not unique but it must only contain one lattice point which implies that the volume of a primitive unit cell is independent of the choice of cell. A consequence of this is that given two different primitive unit cells for the same Bravais lattice it must be possible to cut one into pieces and translate with appropriated lattice vectors into the other and reassemble perfectly and vice versa. We choose for graphene a primitive cell in real space an equilateral parallelogram spanned by the vectors in Eq. (1.15). Another choice could had been the Wigner–Seitz primitive cell which resembles the symmetry of the lattice and is therefore of hexagonal shape. It is constructed by drawing lines from one Bravais lattice point to all its nearest neighbors, cutting each line at half with a plane perpendicular to the line and taking the smallest polyhedron containing the point connected by these planes. The Wigner–Seitz primitive cell we will refer to again when considering the reciprocal lattice of graphene.

Each carbon atom at site A is connected to three nearest neighbors with the aforementioned σ-bonds that all are of type B. Therefore one could say graphene's hexagonal lattice consists of two triangular sublattices consisting of A(red) and B(blue) sites as can be seen in Fig. 1.4(a) along with its other fundamental lattice properties mentioned above.

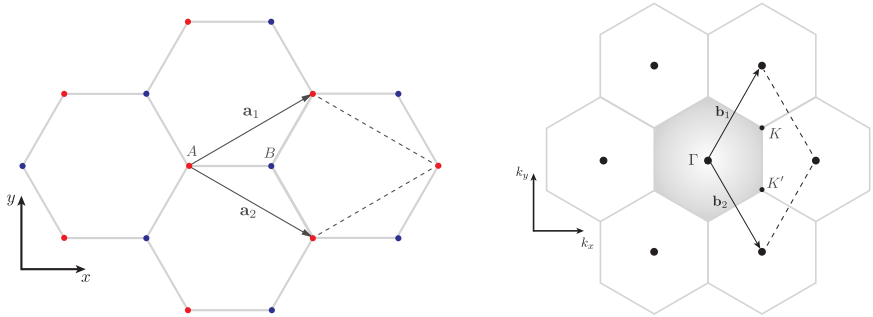

(a) Graphene in real space. The unit cell consisting of two carbon atoms is spanned by the to primitive lattice vectors. The two triangular sublattices can also be seen as red and blue dots.

(b) Graphene in reciprocal space. The first Brillouin zone is shaded and the reciprocal unit cell is spanned by the to primitive reciprocal lattice vectors. Two nonequivalent Dirac points K and K' are shown.

Figure 1.4: Graphene in real and reciprocal space along with its fundamental lattice properties.

Now we turn our attention to the reciprocal lattice which is defined in the following way: Consider a Bravais lattice generated by the lattice vector $\mathbf{R}$ and a plane wave $e^{i\mathbf{k}\cdot\mathbf{r}}$ having some periodicity not necessarily the same as the

lattice. If for some wave vector $\mathbf{K}$

$$e^{i\mathbf{K}\cdot(\mathbf{r}+\mathbf{R})} = e^{i\mathbf{K}\cdot\mathbf{r}}, \tag{1.16}$$

$$\Rightarrow \qquad e^{i\mathbf{K}\cdot\mathbf{R}} = 1 \tag{1.17}$$

is true for any $\mathbf{r}$ and all $\mathbf{R}$ in the lattice then this set of wave vectors $\mathbf{K}$ yielding the periodicity of the lattice is known as the reciprocal lattice. It is a little cumbersome to derive the primitive reciprocal lattice vectors since the cross product used in three-dimensions is not defined in two-dimensions but from a geometrical point of view graphene is of course finite in height but it is negligible compared to its length and width. Therefore we could say that there is a third primitive lattice vector $\mathbf{a}_3$ in real space only having component along the z-axis but vanishing in x and y. Then we also have to add a 0 to the z component of $\mathbf{a}_1$ and $\mathbf{a}_2$. Now we are in stand to find the primitive reciprocal lattice vectors

$$\mathbf{b}_1 = 2\pi \frac{\mathbf{a}_2 \times \mathbf{a}_3}{\mathbf{a}_1 \cdot (\mathbf{a}_2 \times \mathbf{a}_3)} = \left(\frac{2\pi}{\sqrt{3}a}, \frac{2\pi}{a} \right), \tag{1.18a}$$

$$\mathbf{b}_2 = 2\pi \frac{\mathbf{a}_3 \times \mathbf{a}_1}{\mathbf{a}_1 \cdot (\mathbf{a}_2 \times \mathbf{a}_3)} = \left(\frac{2\pi}{\sqrt{3}a}, -\frac{2\pi}{a} \right). \tag{1.18b}$$

The third primitive reciprocal lattice vector $\mathbf{b}_3$ we drop since graphene can be described as effectively being two–dimensional. Now just as for real space in Eq. (1.14) we have a reciprocal lattice vector

$$\mathbf{K} = m_1\mathbf{b}_1 + m_2\mathbf{b}_2, \tag{1.19}$$

where m_1 and m_2 are integers and translations of $\mathbf{K}$ will fill the reciprocal space without overlapping itself or leaving gaps in between. It is obvious that Eq. (1.17) is satisfied as $\mathbf{K}\cdot\mathbf{R} = 2\pi(m_1n_1+m_2n_2)$ since $\mathbf{b}_i\cdot\mathbf{a}_j = 2\pi\delta_{ij}$ per definition. In Fig. 1.4(b) the reciprocal lattice is illustrated along with a reciprocal unit cell spanned by the vectors $\mathbf{b}_1$ and $\mathbf{b}_2$. To get more understanding on the reciprocal lattice we would like to state some additional properties:

- The reciprocal lattice of a given Bravais lattice is always a Bravais lattice itself though not necessary the same Bravais lattice as it was derived from.
- Taking the reciprocal of the reciprocal lattice results in the original Bravais lattice.
- The real lattice is spanned by position vector $\mathbf{R}$ having units of length where as the reciprocal lattice is spanned by reciprocal lattice $\mathbf{K}$ having units of length^{-1}.
- If A is the area of the primitive unit cell in real space then ${}^{(2\pi)^2}/_{A}$ is the area of the reciprocal lattice primitive unit cell.

- The real lattice can be viewed with a high–resolution electron microscope and the reciprocal lattice can be visualized by the diffraction patterns of X–rays.

The Wigner–Seitz primitive cell defined above of the reciprocal lattice is better known as the first Brillouin zone and is very important when considering the dynamics of the electrons in reciprocal space. In Section 2.2 we will find out how two out of six corners of the first Brillouin zone are of high importance when studying the dynamics of the electrons in graphene. [5][8]

1.4.2 History and future of graphene

After having gained knowledge about the fundamental properties of graphene in subsection 1.4.1, we are in stand to understand the history of the development and discovery of these monoatomic crystals which traces back to the early 19th century.

In the 1840s a German scientist, Schafhaeutl, reported that he had inserted small molecule species in between the carbon layers of graphite oxide (GO) and resulting in different graphite intercalation compounds (GICs). The effect of that process was to increase the interlayer spacing between individual carbon layers resulting in electronic decoupling. After having done that, exfoliation was possible with sulfuric and nitric acids. In 1859, the British chemist, Brodie, modified what Schafhaeutl had done before aiming to be able to characterize the molecular weight of graphite by use of strong acids and some oxidants. What he produced was not only intercalation of graphite layers but also chemical oxidation of the surface of graphite, hence generating GO. It turns out that these methods used to modify graphite and obtaining GICs where the forces between graphite layers is reduced and spacing increased are still used today to generate reduced graphite and graphene oxides (r-GO). A long time passed without any major discoveries in producing graphene but in 1962 almost a century after Brodie's publications, Boehm et al., produced thin lamellar graphite from GO that only contained small amounts of oxygen and hydrogen which they had used in the preparation. By using transmission electron microscopy (TEM) they were able to measure the thickness to be 4.6 Å within considerable uncertainties. Nevertheless Boehm concluded that their observation confirmed that the thinnest graphite flakes able to produce were essentially single carbon layers [9].

The story to isolate individual graphite layers continues to be unsuccessful but despite that each attempt was an important step towards the goal which in 2004 was reached by two Russian physicist, Andre Geim and Konstantin Novoselov. The method of success came from a rather unexpected device, namely a scotch tape, probably available in your nearest grocery store. What they did was to use bulk graphite, which consists of large number of graphene layers held together by Van der Waals forces, and then press the adhesive tape onto the graphite crystal thereby removing few layers of graphene. The graphitic flakes now stuck

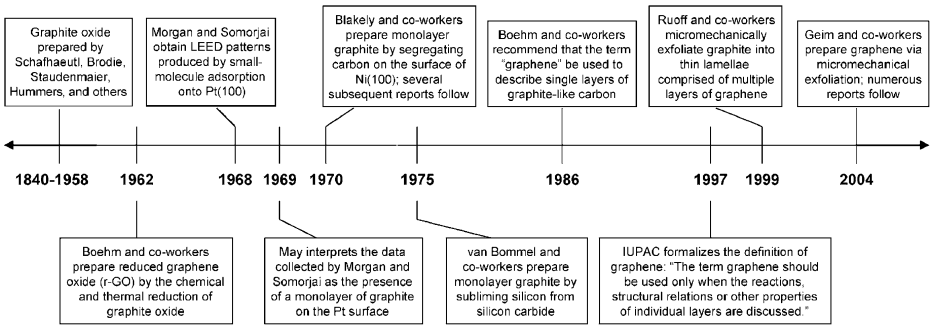

Figure 1.5: Timeline showing important events in the history of producing graphene.[9]

to the adhesive tape were transferred to some substrate by pressing the tape against its surface leaving extremely high-quality examples on top (see Fig. 1.6(a)). Now to identify monolayers of graphite in a pile of multilayer graphite was not an easy task but it turned out that a substrate consisting of Si/SiO_2 with 300 nm layer of SiO_2 made the monolayer crystals in the pile visible as can be seen in Fig. 1.6(b), instead of being transparent as they were on top of some other substrate. Graphene research has exploded since its isolation in 2004 with number of publications exponentially increasing all the time since as can be seen in Fig. 1.7. In 2010 Andre Geim and Konstantin Novoselov were awarded the Nobel Prize in Physics for groundbreaking experiments regarding the two–dimensional material graphene [12].

Regarding the future of graphene it would be nonsense to not say it was bright. At the moment money are being pumped into the graphene research hoping to revolutionize our society from different aspects in the future. Due to graphene's superior properties to other materials for example the mechanical stiffness, strength and elasticity, electrical and thermal conductivity and many more it has the potential to do so. The Graphene Flagship is an European project that aims for planning and structuring the graphene research and making this revolution real. One thing graphene research has also generated is the interest in other 2D atomic crystals making up a whole new branch of science that only deals with the one atomic thick version of bulk materials. [13]

1.5 Motivation for bound state research

In this section we would like take a close look on two specific examples which demonstrate how the effect of electron–electron interaction has lead to new fundamental understanding of properties of materials. In both cases bound states are generated that were not present without the interaction effects.

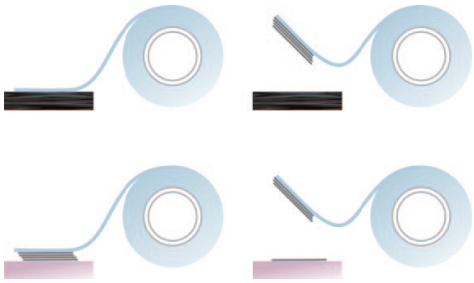

(a) The scotch tape method used to exfoliate graphite to produce individual layers of graphene illustrated.

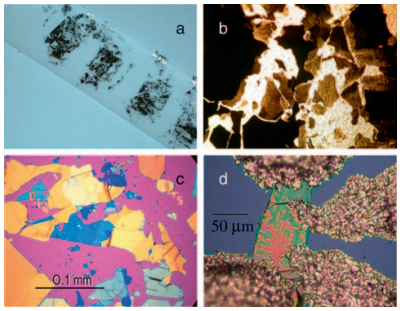

(b) a) HOPG leftovers on scotch tape. b) Graphene flakes. c) Graphene flakes on an oxidized SI wafer. The blue color indicates the most thinnest flakes. d) One of the first devices used to do measurments on graphene.

Figure 1.6: To the left we see an illustration of the amazingly simple scotch tape method. To the right we see the figures of the procedure from generating graphene to measuring its properties.[10][11]

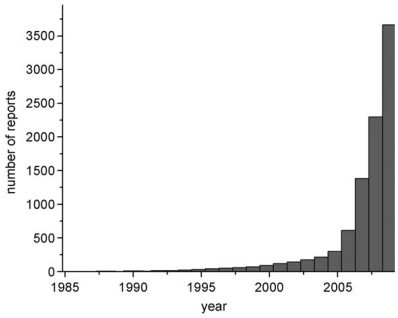

Figure 1.7: From the SciFinder Scholar database. The graph shows number of reports by year containing the searching term "graphene".[9]

1.5.1 Plasmons in the electron gas

Considering non-interacting two-dimensional electron gas the polarization function

$$\chi(\mathbf{r}t, \mathbf{r}'t') = -i\theta(t-t') \left\langle [\rho(\mathbf{r}t), \rho(\mathbf{r}'t')] \right\rangle , \tag{1.20}$$

which is a two–particle correlation function, where $\rho(\mathbf{r}t)$ is the charge operator, can give us information about the dissipation due to an applied field in the following way

$$\mathrm{Re}\,\sigma(\mathbf{q},\omega) = -\frac{\omega e^2}{q^2}\mathrm{Im}\,\chi^R(\mathbf{q},\omega). \tag{1.21}$$

Fourier transforming the polarization function we get to momentum space where Eq. (1.20) takes the form

$$\chi^R(\mathbf{q}, t-t') = -\mathrm{i}\theta(t-t')\frac{1}{\mathcal{V}}\left\langle[\rho(\mathbf{q},t),\rho(-\mathbf{q},t')]\right\rangle. \tag{1.22}$$

It depends only on $\mathbf{q}$ due to the translational invariance of the system and we have written the superscript R for "Retarded" meaning that the function depends on what happened earlier in time. Plugging in the appropriated form of the charge operator where we have attached the trivial phase factor for time evolution since we are dealing with free electrons

$$\rho(\mathbf{q},t) = \sum_{\mathbf{k}\sigma} c^\dagger_{\mathbf{k}\sigma} c_{\mathbf{k}+\mathbf{q}\sigma} \mathrm{e}^{\mathrm{i}(\xi_{\mathbf{k}}-\xi_{\mathbf{k}+\mathbf{q}})t}, \tag{1.23}$$

into Eq. (1.22) we get within the free electron approximation

$$\chi^R_0(\mathbf{q}, t-t') = -\mathrm{i}\theta(t-t')\frac{1}{\mathcal{V}}\sum_{\mathbf{k}\mathbf{k}'}\sum_{\sigma\sigma'}\left[c^\dagger_{\mathbf{k}\sigma}c_{\mathbf{k}+\mathbf{q}\sigma}, c^\dagger_{\mathbf{k}'\sigma'}c_{\mathbf{k}'-\mathbf{q}'\sigma'}\right] \times \mathrm{e}^{\mathrm{i}(\xi_{\mathbf{k}}-\xi_{\mathbf{k}+\mathbf{q}})t}\mathrm{e}^{\mathrm{i}(\xi_{\mathbf{k}'}-\xi_{\mathbf{k}'-\mathbf{q}})t'}. \tag{1.24}$$

At last we would like to go to frequency space which is done by a Fourier transformation, resulting in

$$\chi^R(\mathbf{q},\omega) = \frac{1}{\mathcal{V}}\sum_{\mathbf{k}\sigma}\frac{n_F(\xi_{\mathbf{k}}) - n_F(\xi_{\mathbf{k}+\mathbf{q}})}{\xi_{\mathbf{k}} - \xi_{\mathbf{k}+\mathbf{q}} + \omega + i\eta}. \tag{1.25}$$

The inclusion of an imaginary part of the frequency is a standard trick to make the transform well-defined, in the end of the calculation we let $\eta \to 0^+$ without any consequences. Now following the instructions from Eq. (1.21) we take the imaginary part of Eq. (1.25)

$$-\operatorname{Im}\chi^R(\mathbf{q},\omega) = \frac{\pi}{\mathcal{V}}\sum_{\mathbf{k}\sigma}\left[n_F(\xi_{\mathbf{k}}) - n_F(\xi_{\mathbf{k}+\mathbf{q}})\right]\delta\left(\xi_{\mathbf{k}} - \xi_{\mathbf{k}+\mathbf{q}} + \omega\right). \tag{1.26}$$

What Eq. (1.26) describes is the ability for the electron gas to generate electron–hole pairs due to absorption of the incoming energy. It is basically the density of electron–hole pair excitations as the delta function only gives non-zero outcome when $\omega = \xi_{\mathbf{k}+\mathbf{q}} - \xi_{\mathbf{k}}$ where $\xi_{\mathbf{k}}$ is the energy of hole below the fermi surface and $\xi_{\mathbf{k}+\mathbf{q}}$ is the energy of an excited electron above the fermi surface (assuming $\omega > 0$). It follows then from Eq. (1.21) that the real part of the conductivity decreases as the imaginary part of the polarization function Eq. (1.26) is positive. In Fig. 1.8 we see a schematic drawing of an electron–hole pair generation and a plot of the imaginary part of the polarization function.

Now turning to the interacting case where we will see that this picture changes dramatically and find out that generation of electron–hole pairs is not the only

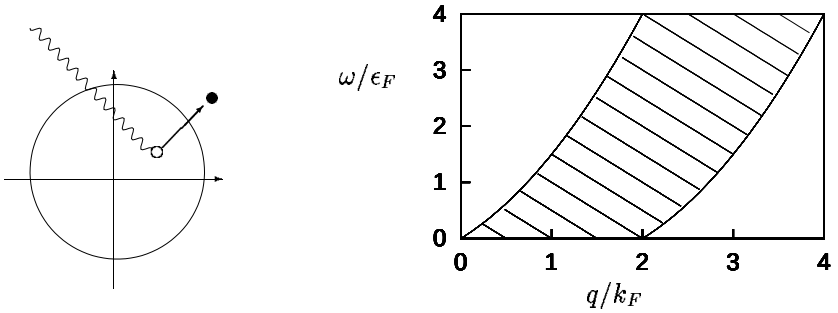

(a) An electron below the Fermi surface absorbs a photon and is excited above, thereby generating an electron–hole pair.

(b) The continuum of electron–hole pairs within in the striped area. Outside no excitations within the non–interaction approximation are allowed.

Figure 1.8: Figures showing the physical origin of how the electron gas dissipates energy when the electrons are considered without interaction.

possible source for dissipation of energy. Let's consider the electron gas being subjected to an external potential in the form of the perturbation

$$\mathcal{H}' = \int \mathrm{d}\mathbf{r}[-e\rho(\mathbf{r})]\phi_{ext}(\mathbf{r},t), \tag{1.27}$$

where $\rho(\mathbf{r})$ now is the particle density. The external potential $\phi_{ext}(\mathbf{q},\omega)$ induces charge density $-e\rho_{ind}(\mathbf{q},\omega)$ which through the Coulomb interaction, $W(\mathbf{q})$, that is present between the electrons corresponds to an induced potential,

$$\phi_{ind}(\mathbf{q},\omega) = \frac{1}{e^2}W(\mathbf{q})[-e\rho_{ind}(\mathbf{q},\omega)]. \tag{1.28}$$

Here all quantities have been Fourier transformed to $(\mathbf{q},\omega)$-space which is allowed due to the translational invariance of the system. Utilizing the Kubo formula which relates the induced charge density with the external potential we can write

$$\phi_{ind}(\mathbf{q},\omega) = W(\mathbf{q})\chi^R(\mathbf{q},\omega)\phi_{ext}(\mathbf{q},\omega), \tag{1.29}$$

where $\chi^R(\mathbf{q},\omega)$ is the Fourier transform of the retarded Kubo density–density correlation function i.e. the same function as we saw in Eq. (1.22). Now we are interested in the total potential which is the sum of the external and internal potential but using Eq. (1.29) allows us to write the total potential entirely as function of the external potential

$$\phi_{tot}(\mathbf{q},\omega) = \phi_{ext}(\mathbf{q},\omega) + \phi_{ind}(\mathbf{q},\omega) \tag{1.30}$$

$$= \left(1 + W(\mathbf{q})\chi^R(\mathbf{q},\omega)\right)\phi_{ext}(\mathbf{q},\omega). \tag{1.31}$$

This is an important result that can best be seen by drawing a parallel to the classical fields **E** and **D** which are connected through the equation $\mathbf{D} = \varepsilon_0 \varepsilon \mathbf{E}$ describing the electric field in a dielectric material. In Eq. (1.31) the total potential corresponds to the electric field **E** and the external potential to the displacement field **D** and therefore we have an expression for the dielectric function $\varepsilon(\mathbf{q}, \omega)$, written as

$$\frac{1}{\varepsilon(\mathbf{q}, \omega)} = 1 + W(\mathbf{q}) \chi^R(\mathbf{q}, \omega). \tag{1.32}$$

The only thing left is to calculate $\chi^R(\mathbf{q}, \omega)$ and then we know $\varepsilon(\mathbf{q}, \omega)$. Without derivation by going through the whole story of including many-body interaction through the powerful Feynman diagram technique we state the random phase approximation result for the dielectric function

$$\varepsilon^{\mathrm{RPA}}(\mathbf{q}, \mathrm{i}q_n) = 1 - W(\mathbf{q}) \chi_0(\mathbf{q}, \mathrm{i}q_n), \tag{1.33}$$

where χ_0 is just the simple pair–bubble diagram and the retarded version of the polarization function can be obtained by analytical continuation $\chi_0^R(\mathbf{q}, \omega) = \chi_0(\mathbf{q}, \mathrm{i}q_n \to \omega + \mathrm{i}\eta)$. Now to study the frequency dependence of the dielectric function in Eq. (1.33), we turn on an external potential with frequency ω. Within the random phase approximation and additionally assuming high frequencies, long wavelengths and low temperatures we are in stand to find an analytical expression for Eq. (1.33), namely

$$\varepsilon^{\mathrm{RPA}}(\mathbf{q}, \omega) = 1 - \frac{\omega_p^2}{\omega} \left(1 + \frac{3}{5} \left(\frac{q v_F}{\omega} \right)^2 \right), \tag{1.34}$$

where we have introduced ω_p, the plasma frequency which is a characteristic frequency for the system given as

$$\omega_p \equiv \sqrt{\frac{n e^2}{m \varepsilon_0}}, \tag{1.35}$$

where n is the electron density, e^2 the electron charge, m the electron mass and ε_0 the electric permittivity constant in vacuum. By considering Eq. (1.31) along with Eq. (1.32) as $\phi_{ext}(\mathbf{q}, \omega) = \varepsilon(\mathbf{q}, \omega) \phi_{tot}(\mathbf{q}, \omega)$ we see that $\varepsilon(\mathbf{q}, \omega) = 0$ actually allows the total potential to vary without any changes in the external potential driving these variations. This corresponds to an oscillatory eigenmode of the system which are called plasma oscillations and are collective charge–charge oscillations. They can be quantized where the quanta are identified as the quasiparticles called plasmons. Implying these conditions in Eq. (1.34) we get

$$\varepsilon^{\mathrm{RPA}}(\mathbf{q}, \omega) = 0, \tag{1.36}$$

$$\Rightarrow \qquad \omega(q) \simeq \omega_p + \frac{3}{10} \frac{v_F^2}{\omega_p} q^2. \tag{1.37}$$

The remarkable fact about these oscillations is that they are not damped because in the high frequency limit $\mathrm{Im}\chi_0^R$ is automatically zero meaning that these plasmons do not find them self in the continuum of electron–hole pairs like we saw in Fig. 1.8. The dispersion relation for plasmons in Eq. (1.37) along with electron–hole continuum can be seen in Fig. 1.9.

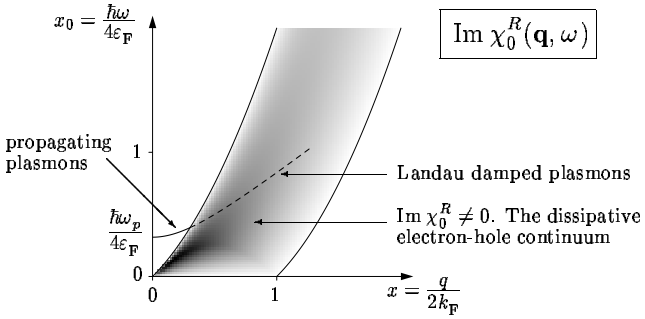

Figure 1.9: The electron–hole continuum giving rise to dissipation when considering non–interacting electron gas along with the plasmon dispersion relation. For small q-values the plasmons have infinite lifetime but acquire finite lifetime when the branch hits the continuum.

To summarize: When considering the non–interacting electron gas the only form of dissipation was the generation of electron–hole pairs. When turning on the interaction we found out for small q-values some of the electron–hole pairs were dragged out of the continuum making and therefore gained infinite lifetime. This is what we call a bound state of electron-hole pairs which in this case are also called plasmons. [14]

1.5.2 Stoner excitations

Another example that motivates the research of bound state formation in graphene is the Stoner theory of ferromagnetism which is a mean-field theory for itinerant ferromagnets. The Hamiltonian describing our system consisting of conduction electrons in one band which is spin-split in the absence of a magnetic field is a Hubbard Hamiltonian

$$\mathcal{H} = \sum_{\mathbf{k}\sigma} \epsilon_{\mathbf{k}} a^\dagger_{\mathbf{k}\sigma} a_{\mathbf{k}\sigma} + \frac{1}{2}\frac{U}{N} \sum_{\mathbf{k}_1\mathbf{k}_2\mathbf{q}} \sum_{\sigma\sigma'} a^\dagger_{\mathbf{k}_1+\mathbf{q}\sigma} a^\dagger_{\mathbf{k}_2-\mathbf{q}\sigma'} a_{\mathbf{k}_2\sigma'} a_{\mathbf{k}_1\sigma}. \tag{1.38}$$

Having a ferromagnetic ground state we want to study the energies for the elementary excitations appearing from that state. That we do by working on the ground state $|\psi_{GS}\rangle$ with an operator that is a linear combination of operators which transfers on electron from state $|\mathbf{k}\uparrow\rangle$ to $|\mathbf{k}+\mathbf{q}\downarrow\rangle$ i.e.

$$\sigma_{\mathbf{q}\mathbf{k}-} = a^\dagger_{\mathbf{k}+\mathbf{q}\downarrow} a_{\mathbf{k}\uparrow}, \tag{1.39}$$

thus generating a state

$$|\psi_{\mathbf{q}}\rangle = \sum_{\mathbf{k}} f_{\mathbf{k}} \sigma_{\mathbf{qk}-} |\psi_{GS}\rangle. \tag{1.40}$$

The $-$ index on the σ-operator indicates we are reducing the total spin by 1 as we annihilate an electron with spin $\uparrow$ and create another with spin $\downarrow$ and $f_{\mathbf{k}}$ are coefficients specifying the linear combination. Eq. (1.40) must fulfill the Schrödinger equation

$$\mathcal{H}|\psi_{\mathbf{q}}\rangle = E|\psi_{\mathbf{q}}\rangle, \tag{1.41}$$

and we get

$$\mathcal{H} \sum_{\mathbf{k}} f_{\mathbf{k}} \sigma_{\mathbf{qk}-} |\psi_{GS}\rangle = (E_{GS} + \hbar\omega_{\mathbf{q}}) \sum_{\mathbf{k}} f_{\mathbf{k}} \sigma_{\mathbf{qk}-} |\psi_{GS}\rangle, \tag{1.42}$$

where we have split the energy on the right hand side in Eq. (1.41) up in two parts, namely the ground state energy E_{GS} and the excitation energy measured from the ground state $\hbar\omega_{\mathbf{q}}$. To find the excitation energy we project onto Eq. (1.42) with the the "bra", $\langle\psi_{GS}|(\sigma_{\mathbf{qk}-})^{\dagger}$, which enables us to obtain the eigenvalue equation determining the excitation energy $\hbar\omega_{\mathbf{q}}$

$$1 = \frac{U}{N} \sum_{\mathbf{k}} \frac{n_{\mathbf{k}\uparrow}(1 - n_{\mathbf{k}+\mathbf{q}\downarrow})}{\epsilon_{\mathbf{k}+\mathbf{q}} - \epsilon_{\mathbf{k}} + 2\mu_B H + \frac{N_e}{N} U\zeta - \hbar\omega_{\mathbf{q}}}. \tag{1.43}$$

The nominator contains number operators in $\mathbf{k}\uparrow$ and $\mathbf{k}+\mathbf{q}\downarrow$ which are present because on the way obtaining Eq. (1.43) we had to evaluate a commutator between $\sigma_{\mathbf{qk}-}$ and $\mathcal{H}_U$ where $\mathcal{H}_U$ is the Coulomb interaction of Hubbard type from Eq. (1.38). This commutator generated products of four second quantization operators that with the help of the random phase approximation were truncated into the number operators in Eq. (1.43) and therefore an analytical solution is possible. In the denominator of the same equation a term due an external magnetic field $2\mu_B H$ is added and the variable ζ is a number between 0 and 1 measuring how many of the total electrons N_e have spin $\uparrow$ so when $\zeta = 0 \rightarrow N_\uparrow = {}^1\!/_2 N_e$ and $\zeta = 1 \rightarrow N_\uparrow = N_e$. To determine the eigenvalues $\hbar\omega_{\mathbf{q}}$ we set the denominator of Eq. (1.43) to zero under the conditions the nominator remains non-zero giving i.e. the state $|\mathbf{k}\uparrow\rangle$ is occupied and $|\mathbf{k}-\mathbf{q}\downarrow\rangle$ is unoccupied. The eigenvalue equation becomes

$$\hbar\omega_{\mathbf{q},\mathbf{k}} = \epsilon_{\mathbf{k}+\mathbf{q}} - \epsilon_{\mathbf{k}} + 2\mu_B H + \frac{N_e}{N} U\zeta. \tag{1.44}$$

These excitations are known as Stoner excitations which are nothing but electron–hole excitations form a continuous band in $(\hbar\omega, q)$-space as can be seen in Fig. 1.10(b). For $q = 0$ the band starts out at Δ defined as

$$\Delta = 2\mu_B H + \frac{N_e}{N} U\zeta, \tag{1.45}$$

which for the special case of no external magnetic field $H = 0$ equals the exchange splitting i.e. $\Delta(H = 0) = \Delta_{ex} = {}^{N_e}\!/_N U\zeta$. On Fig. 1.10(a) we see the the density of states and the two spin-split bands of Δ.

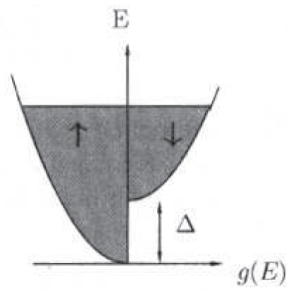

(a) The density of states and the splitting of the two spin bands in the Stoner theory.[3]

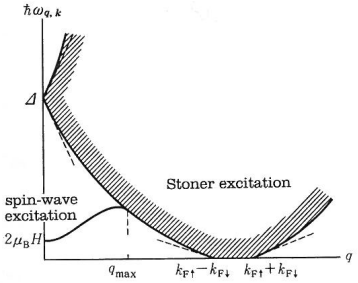

(b) The stoner excitations and the dispersion relation for spin waves which exists outside the continuum and represents therefore long living collective excitations.[15]

Figure 1.10: The density of states in the Stoner theory and the Stoner excitations along with the spin wave dispersion relation.

What now becomes very interesting is the fact in the window below the Stoner excitations the interaction drives some of the electron–hole pairs out of the continuum forming a mode of long living collective excitations called spin–wave excitations. The energy dispersion for these excitations starts out at $2\mu_B H$ for $q = 0$ and is proportional to q^2 for small q. At $q = q_{max}$ the mode merges into the continuum and does not represent long living excitation anymore.[15]

Again we have seen that the interaction between electrons is responsible in formation of bound states in the material which in this case is a ferromagnet. The long living excitations are spin waves and can be quantized and called magnons. They are magnetic as the name suggests because they spin have 1.

Chapter 2

The Hubbard model

In this chapter we will discuss the Hubbard model in general and then analyze each term carefully in the case for graphene. We will obtain the dispersion relation and derive its linear form but most importantly we will transform the interaction to k-space and see how it appears there.

2.1 General remarks on the Hubbard model

In the early 1960's John Hubbard et al. designed a model to understand the behaviour of transition metal monoxides (FeO, NiO, CoO) which takes into account the quantum mechanical motion of electrons in solids and the non-trivial repulsive Coulomb interaction between electrons. The model captures the low energy physics of the strongly interacting electrons in solids by successfully eliminating the high energy degrees of freedom by the renormalization method. Despite its simplicity it reveals the dynamics and behaviour of diverse complex system ranging from metal–insulator transitions and antiferromagnetism to high temperature superconductivity. The Hubbard model is written as

$$\mathcal{H} = \mathcal{H}_{TB} + \mathcal{H}_U, \tag{2.1}$$

so it only consists of two terms, the former is the tight-binding term or the kinetic energy term describing the hopping of the electrons in the lattice whereas the latter term describes the interaction between the electrons. Analyzing each term separately is easy but combined is difficult since the terms do not commute. The Hamiltonian also reveals the wave–particle duality of quantum mechanics where the tight-binding term describes waves but the interaction term describes particles. The sum therefore becomes a competition between the two effects where the results depends on the system under consideration. [16][17]

2.2 Tight-binding model of graphene

Having gone through the basic properties of graphene in Section 1.4.1 we know that the electrons in the p_z orbitals are loosely bound to the nuclei of each carbon atom. They become delocalized and are responsible for the electronic properties of graphene. We are though still in position to use the tight-binding approximation on the problem since the overlap between the p_z orbitals on neighbouring atoms is small enough to obtain an approximate analytical expression for the band structure.

In the tight-binding method we construct a wave function that is a linear combination of atomic orbitals of all the atoms in the lattice. The Hamiltonian for a single electron in the potential of all the carbon atoms in graphene is given by

$$\mathcal{H}_{\text{crystal}} = \mathcal{H}_{\text{kinetic}} + V_{\text{atoms}}, \tag{2.2}$$

where the $\mathcal{H}_{\text{kinetic}} = \hat{p}^2/2m_e$ is the usual kinetic energy operator and V_{atoms} is the potential from all the carbon atoms in the lattice. Due to the periodicity of the lattice we expect the wave functions to fulfill Bloch's theorem which states that the eigenstate of a particle in a periodic potential may be written as the product of a plane wave and a periodic function that has the same periodicity as the lattice. They are

$$|\psi_{\mathbf{k}}\rangle = \frac{1}{\sqrt{N}} \sum_i \mathrm{e}^{\mathrm{i}\mathbf{k}\cdot\mathbf{R}_i} |\phi\rangle, \tag{2.3}$$

where the sum is over all R_i which connects all the N unit cells. $|\psi_{\mathbf{k}}\rangle$ is a bra(c)ket notation for $\psi_{\mathbf{k}}(\mathbf{r})$ and the periodic function $|\phi\rangle = \phi(\mathbf{r} - \mathbf{R}_i)$ is a so called Wannier function and does not have to be an exact atomic wave function but in general is a sum over all appropriated exact atomic orbitals. Having discussed the atomic orbitals of graphene before we recognize $|\phi\rangle$ therefore as the relevant p_z orbital of the carbon atoms. It is clear that Eq. (2.3) satisfies Bloch's theorem which states that $\psi(\mathbf{r}+\mathbf{R}) = \mathrm{e}^{\mathrm{i}\mathbf{k}\cdot\mathbf{R}}\psi(\mathbf{r})$ for all $\mathbf{R}$ in the Bravais lattice

$$\psi_{\mathbf{k}}(\mathbf{r}+\mathbf{R}) = \frac{1}{\sqrt{N}} \sum_i \mathrm{e}^{\mathrm{i}\mathbf{k}\cdot\mathbf{R}_i} \phi(\mathbf{r}+\mathbf{R}-\mathbf{R}_i) \tag{2.4}$$

$$= \mathrm{e}^{\mathrm{i}\mathbf{k}\cdot\mathbf{R}} \frac{1}{\sqrt{N}} \sum_i \mathrm{e}^{\mathrm{i}\mathbf{k}\cdot(\mathbf{R}_i-\mathbf{R})} \phi(\mathbf{r}-(\mathbf{R}_i-\mathbf{R})) \tag{2.5}$$

$$= \mathrm{e}^{\mathrm{i}\mathbf{k}\cdot\mathbf{R}} \psi_{\mathbf{k}}(\mathbf{r}). \tag{2.6}$$

In addition the Bloch functions must obey the periodic boundary conditions

$$\psi_{\mathbf{k}}(\mathbf{r} + N_i\mathbf{a}_i) = \psi_{\mathbf{k}}(\mathbf{r}), \qquad i = 1, 2, \tag{2.7}$$

where $\mathbf{a}_i$ are the primitive lattice vectors Eq. (1.15) and $N_i \sim \sqrt{N}$ with N the

total number of unit cells as before. Using Bloch's theorem on Eq. (2.7) gives

$$\psi_{\mathbf{k}}(\mathbf{r} + N_i\mathbf{a}_i) = \mathrm{e}^{\mathrm{i}N_i\mathbf{k}\cdot\mathbf{a}_i}\psi_{\mathbf{k}}(\mathbf{r}), \tag{2.8}$$

$$\Rightarrow \qquad \mathrm{e}^{\mathrm{i}N_i\mathbf{k}\cdot\mathbf{a}_i} = 1, \tag{2.9}$$

which determines the allowed k values

$$k_x = \frac{2\pi}{N_1 a_1} p_x, \qquad p_x = 0, 1, \cdots, N_1 - 1, \tag{2.10a}$$

$$k_y = \frac{2\pi}{N_2 a_2} p_y, \qquad p_y = 0, 1, \cdots, N_2 - 1. \tag{2.10b}$$

In general the Bloch wave vector can be written as

$$\mathbf{k} = \frac{p_x}{N_1}\mathbf{b}_1 + \frac{p_y}{N_2}\mathbf{b}_2, \qquad p_x = p_y = 0, 1, \cdots, N_x - 1 = N_y - 1 \tag{2.11}$$

from where we can conclude that the volume $\Delta\mathbf{k}$ in k–space that each allowed value of $\mathbf{k}$ occupies is the volume of the parallelepiped spanned by $\mathbf{b}_1/N_1$, $\mathbf{b}_2/N_2$ and $\mathbf{b}_3/N_3$,

$$\Delta\mathbf{k} = \frac{\mathbf{b}_1}{N_1} \cdot \left(\frac{\mathbf{b}_2}{N_2} \times \frac{\mathbf{b}_3}{N_3} \right) \tag{2.12}$$

$$= \frac{1}{N}\, \mathbf{b}_1 \cdot \mathbf{b}_2 \times \mathbf{b}_3. \tag{2.13}$$

Again we have used the trick to include the third dimension of graphene by adding in real space an unit vector $\mathbf{a}_3$ in the z direction to be able to calculate properties of the effectively two–dimensional plane. $\mathbf{b}_1 \cdot \mathbf{b}_2 \times \mathbf{b}_3$ is then the volume of the reciprocal primitive cell with height corresponding to one layer of carbon atoms so therefore N_3=1 in Eq. (2.13). $\Delta\mathbf{k}$ we therefore recognize as effectively the area of the parallelogram spanned by $\mathbf{b}_1$ and $\mathbf{b}_2$. Most importantly Eq. (2.13) states that the number of allowed wave vectors in the first Brillouin zone is equal to the number of unit cells in the crystal. Since any wave vector $\mathbf{k}$ can be transferred into the first Brillouin zone by a reciprocal lattice vector all unique values of $\mathbf{k}$ can be found there. The transfer of wave vectors is allowed because some $\mathbf{k}'$ outside the first Brillouin zone can be written as $\mathbf{k}' = \mathbf{k} + \mathbf{K}$ where $\mathbf{k}$ is inside the first Brillouin zone and $\mathbf{K}$ is a reciprocal lattice vector. Therefore we have reduced the original problem of finding the energy dispersion of an electron in a potential of N carbon atoms to a simpler one namely N independent problems for each allowed value of $\mathbf{k}$ within the first Brillouin zone.[8]

The wave functions that fulfill all the above-mentioned criteria are

$$|\psi_{\mathbf{k}}\rangle = \frac{1}{\sqrt{N}} \sum_i \mathrm{e}^{\mathrm{i}\mathbf{k}\cdot\mathbf{R}_i} \left(u_{\mathbf{k}} |iA\rangle + v_{\mathbf{k}} |iB\rangle \right), \tag{2.14}$$

where $u_{\mathbf{k}}$ and $v_{\mathbf{k}}$ are in general complex numbers depending on wave vector $\mathbf{k}$. $|iA\rangle$ and $|iB\rangle$ are p_z atomic orbitals centered at atom A and B respectively in

unit cell i.

We find the eigenvalues and eigenfunctions by solving the Schrödinger equation for the full Hamiltonian

$$\mathcal{H}_{Crystal}|\psi_{\mathbf{k}}\rangle = E_{\mathbf{k}}|\psi_{\mathbf{k}}\rangle. \tag{2.15}$$

By projecting onto Eq. (2.15) with arbitrary states $\langle jA|$ and $\langle jB|$ denoting atoms at sites A and B in unit cell j and write the results in matrix form we get

$$\begin{pmatrix} \mathcal{H}_{AA} & \mathcal{H}_{AB} \\ \mathcal{H}_{BA} & \mathcal{H}_{BB} \end{pmatrix} \begin{pmatrix} u_{\mathbf{k}} \\ v_{\mathbf{k}} \end{pmatrix} = E_{\mathbf{k}} \begin{pmatrix} \mathcal{S}_{AA} & \mathcal{S}_{AB} \\ \mathcal{S}_{BA} & \mathcal{S}_{BB} \end{pmatrix} \begin{pmatrix} u_{\mathbf{k}} \\ v_{\mathbf{k}} \end{pmatrix}, \tag{2.16}$$

where $\mathcal{H}$ are called the transfer integral matrix having units of energy and and $\mathcal{S}$ the overlap integral matrix which is dimensionless. The matrix elements are defined as

$$\mathcal{H}_{\alpha\beta} = \frac{1}{N}\sum_i \mathrm{e}^{\mathrm{i}\mathbf{k}\cdot\mathbf{R}_i}\langle j\alpha|\mathcal{H}|i\beta\rangle, \tag{2.17}$$

$$\mathcal{S}_{\alpha\beta} = \frac{1}{N}\sum_i \mathrm{e}^{\mathrm{i}\mathbf{k}\cdot\mathbf{R}_i}\langle j\alpha|i\beta\rangle. \tag{2.18}$$

Now looking at each element in Eq. (2.16) we can infer that the diagonal elements of both the transfer integral matrix and the overlap matrix are equivalent i.e. $\mathcal{H}_{AA} = \mathcal{H}_{BB}$ and $\mathcal{S}_{AA} = \mathcal{S}_{BB}$, since the two carbon atoms in the unit cell are identical. Additionally the off-diagonal elements correspond to physical observables and should therefore be the hermitian conjugate of each other within each matrix i.e. $\mathcal{H}_{AB} = \mathcal{H}^*_{BA}$ and $\mathcal{S}_{AB} = \mathcal{S}^*_{BA}$.

Now using a nearest neighbour approximation which states that the atomic orbital of an electron in any unit cell only overlaps with the atomic orbital of its nearest neighbors. In graphene (see Fig. 1.4(a)) each atom at site A has three nearest neigbors all placed at site B in distinct unit cells so the diagonal elements of the transfer integral matrix are just the energies of the p_z orbitals centered at each atom. Since we are working with the full crystal hamiltonian this energy is not the exact energy as if the atom is isolated but close to. At last since we are free to choose our own reference point of energy so we set these elements to zero. Now winding the story back to the off-diagonal elements of the transfer integral matrix what we get when using the nearest neighbour approximation is

$$\mathcal{H}_{AB} = \frac{1}{N}\sum_i \mathrm{e}^{\mathrm{i}\mathbf{k}\cdot\mathbf{R}_i}\langle jA|\mathcal{H}|iB\rangle \tag{2.19}$$

$$= \frac{1}{N}\sum_i \left(1 + \mathrm{e}^{-\mathrm{i}\mathbf{k}\cdot\mathbf{a}_1} + \mathrm{e}^{-\mathrm{i}\mathbf{k}\cdot\mathbf{a}_2}\right)(-t) \tag{2.20}$$

$$= -tf(\mathbf{k}). \tag{2.21}$$

Again because each atom at site A is connected to three atoms at site B and vice versa we get three terms in Eq. (2.20), the first term is due the atom in the same unit cells and the two latter terms are due to the atoms in the neighbouring unit cells connected by lattice vectors $\mathbf{a}_1$ and $\mathbf{a}_2$. We also define the hopping integral $t \equiv -\langle jA|\mathcal{H}|iB\rangle = -\langle jB|\mathcal{H}|iA\rangle$ which is the energy required to hop from one site to another neighbouring site and is assumed to be real.

There will be a similar off-diagonal element for the overlap integral matrix but according to experiments it is approximately an order of magnitude lower than t which is $\sim 2.8\,\mathrm{eV}$ so in this thesis we neglect these elements and consequently the overlap integral matrix is just the 2×2 identity matrix $\mathcal{I}_2$.

Now Eq. (2.16) can be written as

$$\begin{pmatrix} 0 & -tf(\mathbf{k}) \\ -tf^*(\mathbf{k}) & 0 \end{pmatrix} \begin{pmatrix} u_\mathbf{k} \\ v_\mathbf{k} \end{pmatrix} = E_\mathbf{k} \begin{pmatrix} u_\mathbf{k} \\ v_\mathbf{k} \end{pmatrix}, \tag{2.22}$$

where

$$f(\mathbf{k}) = 1 + \mathrm{e}^{-\mathrm{i}\mathbf{k}\cdot\mathbf{a}_1} + \mathrm{e}^{-\mathrm{i}\mathbf{k}\cdot\mathbf{a}_2}. \tag{2.23}$$

Finding the eigenvalues corresponds to solving the secular equation, $\det(\mathcal{H} - E\mathcal{I}_2) = 0$, yielding two eigenenergies

$$E_{\mathbf{k}\pm} = \pm t|f(\mathbf{k})| \tag{2.24}$$

$$= \pm t\sqrt{1 + 4\cos\left(\frac{\sqrt{3}ak_x}{2}\right)\cos\left(\frac{ak_y}{2}\right) + \cos^2\left(\frac{ak_y}{2}\right)}, \tag{2.25}$$

where the positive solution is referred to as the conduction band and the negative solution as the valence band. Graphical illustrations of the Eq. (2.25) can both be seen in Fig. 2.1 as contourplot and in Fig. 2.2 in 3D version.
The two eigenvalues have corresponding eigenvectors

$$\begin{pmatrix} u_\mathbf{k} \\ v_\mathbf{k} \end{pmatrix}_\pm = \frac{1}{\sqrt{2}} \begin{pmatrix} \mp\frac{f(\mathbf{k})}{|f(\mathbf{k})|} \\ 1 \end{pmatrix} \tag{2.26}$$

$$= \frac{1}{\sqrt{2}} \begin{pmatrix} \mp\mathrm{e}^{\mathrm{i}\phi_\mathbf{k}} \\ 1 \end{pmatrix}, \tag{2.27}$$

$$\text{where} \quad \phi_\mathbf{k} = \mathrm{Arg}(f(\mathbf{k})). \tag{2.28}$$

For later usage we want to multiply the eigenvector referring to positive energy by a complex number $\mathrm{e}^{-\mathrm{i}\phi_\mathbf{k}}$ of length $|\mathrm{e}^{-\mathrm{i}\phi_\mathbf{k}}| = 1$. This operation should not affect the physical results because according to the fundamental rules of quantum mechanics a state is represented by a vector and another vector having same

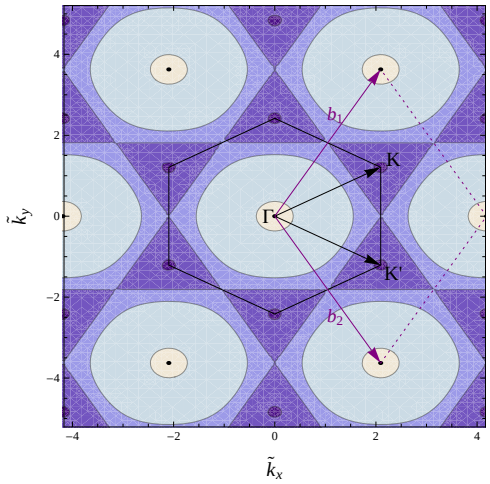

Figure 2.1: The dispersion relation as contourplot. The first Brillouin zone, a reciprocal unit cell spanned by the reciprocal lattice vectors and the two nonequivalent points $\mathbf{K}$ and $\mathbf{K}'$ are superimposed.

direction represents the same state. We get

$$\begin{pmatrix} u_{\mathbf{k}} \\ v_{\mathbf{k}} \end{pmatrix}_+ = \frac{1}{\sqrt{2}} \begin{pmatrix} -\mathrm{e}^{\mathrm{i}\phi_{\mathbf{k}}} \\ 1 \end{pmatrix} \rightarrow \begin{pmatrix} u_{\mathbf{k}} \\ v_{\mathbf{k}} \end{pmatrix}_+ = \frac{1}{\sqrt{2}} \begin{pmatrix} -\mathrm{e}^{\mathrm{i}\phi_{\mathbf{k}}} \\ 1 \end{pmatrix} \cdot \mathrm{e}^{-\mathrm{i}\phi_{\mathbf{k}}} \tag{2.29}$$

$$= \frac{1}{\sqrt{2}} \begin{pmatrix} -1 \\ \mathrm{e}^{-\mathrm{i}\phi_{\mathbf{k}}} \end{pmatrix}. \tag{2.30}$$

In Fig. 2.2 the energy dispersion relation Eq. (2.25) is plotted in reciprocal space and in Fig. 2.1 we have a contourplot of the same dispersion relation where the first Brillouin zone is shown along with a parallelogram reciprocal unit cell. What is to be noticed is that conduction band and valence band touch at the six corners of the hexagonal Brillouin zone. These six points form two sets of three equivalent points since one can get from one corner to another within each set by a reciprocal lattice vector. We choose one point from each set and denote them K and K' having coordinates

$$\mathbf{K} = \left(\frac{2\pi}{\sqrt{3}a}, \frac{2\pi}{3a} \right), \tag{2.31a}$$

$$\mathbf{K}' = \left(\frac{2\pi}{\sqrt{3}a}, -\frac{2\pi}{3a} \right). \tag{2.31b}$$

At these specific points the energy dispersion can be linearized which is what can be seen in Fig. 2.2 and detailed calculations in Section 2.3.

The Fermi energy is defined as the energy of the electron sitting in the highest occupied k-state when the solid is in its ground state at $T = 0$. Since electrons

are fermions and obey Pauli's exclusion principle, stating that no fermions can share all the same quantum numbers, we populate k-space from the lowest possible state and upwards, just as filling a bucket with water. There are N k-states, as many as unit cells in each band, that can accommodate $2N$ electrons taking spin degeneracy into account. Having two atoms in each unit cell of graphene, therefore results in a filled valence band and an empty conduction band. Due to this, graphene is referred to as being a semimetal or zero–gap semiconductor with value of Fermi energy defined to be $E_F = 0$. Now having solved the eigenvalue problem for the two band tight-binding model and gotten the appropriated form of the eigenvectors we can plug the eigenvector corresponding to the negative eigenvalue from Eq. (2.27) and the eigenvector corresponding to the positive eigenvalue from Eq. (2.30) into the original wave function Eq. (2.14). Written in matrix form it yields

$$\begin{pmatrix} |\psi_{\mathbf{k}+}\rangle \\ |\psi_{\mathbf{k}-}\rangle \end{pmatrix} = \frac{1}{\sqrt{N}} \sum_i \mathrm{e}^{\mathrm{i}\mathbf{k}\cdot\mathbf{R}_i} \frac{1}{\sqrt{2}} \begin{pmatrix} -1 & \mathrm{e}^{-\mathrm{i}\phi_{\mathbf{k}}} \\ \mathrm{e}^{\mathrm{i}\phi_{\mathbf{k}}} & 1 \end{pmatrix} \begin{pmatrix} |iA\rangle \\ |iB\rangle \end{pmatrix} \tag{2.32}$$

$$= \frac{1}{\sqrt{N}} \sum_i \mathrm{e}^{\mathrm{i}\mathbf{k}\cdot\mathbf{R}_i} \underline{\underline{U_{\mathbf{k}}}} \begin{pmatrix} |iA\rangle \\ |iB\rangle \end{pmatrix}, \tag{2.33}$$

$$\text{where} \quad \underline{\underline{U_{\mathbf{k}}}} \equiv \frac{1}{\sqrt{2}} \begin{pmatrix} -1 & \mathrm{e}^{-\mathrm{i}\phi_{\mathbf{k}}} \\ \mathrm{e}^{\mathrm{i}\phi_{\mathbf{k}}} & 1 \end{pmatrix}. \tag{2.34}$$

Adopting second quantization notation where a state vector is substituted by a operator $c^\dagger$ that can create a particle with certain quantum numbers when working on a empty state. In that language we get

$$\begin{pmatrix} c^\dagger_{\mathbf{k}+} \\ c^\dagger_{\mathbf{k}-} \end{pmatrix} = \frac{1}{\sqrt{N}} \sum_i \mathrm{e}^{\mathrm{i}\mathbf{k}\cdot\mathbf{R}_i} \underline{\underline{U_{\mathbf{k}}}} \begin{pmatrix} c^\dagger_{iA} \\ c^\dagger_{iB} \end{pmatrix}. \tag{2.35}$$

The task is to diagonalize the tight-binding hamiltonian in k-space so therefore we want to invert Eq. (2.39) i.e. find how creating a particle at site A/B in unit cell i corresponds to a linear combination of creating a particle with wave vector $\mathbf{k}$ having positive energy and creating a particle with wave vector $\mathbf{k}$ having negative energy. What we do is multiplying by $1/\sqrt{N}$, $\sum_{\mathbf{k}} \mathrm{e}^{-\mathrm{i}\mathbf{k}\cdot\mathbf{R}_j}$ and $\underline{\underline{U_{\mathbf{k}}}}^{-1}$ on both sides giving

$$\frac{1}{\sqrt{N}} \sum_{\mathbf{k}} \mathrm{e}^{-\mathrm{i}\mathbf{k}\cdot\mathbf{R}_j} \underline{\underline{U_{\mathbf{k}}}}^{-1} \begin{pmatrix} c^\dagger_{\mathbf{k}+} \\ c^\dagger_{\mathbf{k}-} \end{pmatrix} = \frac{1}{N} \sum_i \sum_{\mathbf{k}} \mathrm{e}^{\mathrm{i}\mathbf{k}\cdot(\mathbf{R}_i - \mathbf{R}_j)} \begin{pmatrix} c^\dagger_{iA} \\ c^\dagger_{iB} \end{pmatrix}. \tag{2.36}$$

Now we use on the right-hand side a standard identity from Fourier analysis which states that

$$\sum_{\mathbf{k}} \mathrm{e}^{\mathrm{i}\mathbf{k}\cdot(\mathbf{R}_i - \mathbf{R}_j)} = N\delta_{i,j}, \tag{2.37}$$

to obtain

$$\begin{pmatrix} c^\dagger_{iA} \\ c^\dagger_{iB} \end{pmatrix} = \frac{1}{\sqrt{N}} \sum_{\mathbf{k}} \mathrm{e}^{-\mathrm{i}\mathbf{k}\cdot\mathbf{R}_i} \underline{\underline{U_{\mathbf{k}}}}^{-1} \begin{pmatrix} c^\dagger_{\mathbf{k}+} \\ c^\dagger_{\mathbf{k}-} \end{pmatrix}. \tag{2.38}$$

In addition we introduce two new indices, sublattice index $\alpha = A/B$ and band index $\beta = +/-$ thereby Eq. (2.38) can be written in a very compact form

$$c^\dagger_{i\alpha\sigma} = \frac{1}{\sqrt{N}} \sum_{\mathbf{k}\beta} \mathrm{e}^{-\mathrm{i}\mathbf{k}\cdot\mathbf{R}_i} U^{-1}_{\mathbf{k}\alpha\beta} c^\dagger_{\mathbf{k}\beta\sigma}, \tag{2.39}$$

where the spin index $\sigma = \{\uparrow, \downarrow\}$ has also been implemented on the operators. The number $U^{-1}_{\mathbf{k}\alpha\beta}$ is now an element of the matrix $\underline{\underline{U_\mathbf{k}}}^{-1}$. For sake of clarity let's write out what is to be understood

$$\underline{\underline{U_\mathbf{k}}}^{-1} = \underline{\underline{U_\mathbf{k}}} \tag{2.40}$$

$$= \frac{1}{\sqrt{2}} \begin{pmatrix} U_{\mathbf{k}A+} & U_{\mathbf{k}B+} \\ U_{\mathbf{k}A-} & U_{\mathbf{k}B-} \end{pmatrix} \tag{2.41}$$

$$= \frac{1}{\sqrt{2}} \begin{pmatrix} -1 & \mathrm{e}^{-\mathrm{i}\phi_\mathbf{k}} \\ \mathrm{e}^{\mathrm{i}\phi_\mathbf{k}} & 1 \end{pmatrix}, \tag{2.42}$$

where the equal sign in Eq. (2.40) is due to that $\underline{\underline{U_\mathbf{k}}}$ is unitary. In this basis the tight-binding hamiltonian is diagonal and can be written as

$$\mathcal{H}_{TB} = \sum_{\mathbf{k}\beta\sigma} \epsilon_{\mathbf{k}\beta} c^\dagger_{\mathbf{k}\beta\sigma} c_{\mathbf{k}\beta\sigma} \tag{2.43}$$

where $\epsilon_{\mathbf{k}\beta} \equiv E_{\mathbf{k}\beta}$ are the energy dispersion relations given in Eq. (2.25).

2.3 Linearization of dispersion relation

A much simpler expression for the dispersion relation in Eq. (2.25) can be obtained by expansion around the Fermi energy in k-space i.e. around $\mathbf{K}$ and $\mathbf{K}'$. We use the coordinates given in Eq. (2.31) but imply the notation $\mathbf{K}(\mathbf{K}') = \left(\frac{2\pi}{\sqrt{3}a}, s\frac{2\pi}{3a}\right)$ where $s = 1(-1)$ for the two nonequivalent corner points of the first Brillouin zone shown in Fig. 2.1. What we do is to write $\mathbf{k} = \mathbf{K}(\mathbf{K}') + \delta\mathbf{k}$ where $\delta\mathbf{k} = (\delta k_x, \delta k_y)$. In the vicinity of $\mathbf{K}(\mathbf{K}')$ the energy dispersion relation can be written as $\epsilon_{\mathbf{k}\pm} = \epsilon_{\delta\mathbf{k}\pm} = \pm|f(\mathbf{K}(\mathbf{K}') + \delta\mathbf{k}))|$ since $\epsilon_{\mathbf{K}(\mathbf{K}')\pm} = 0$. What we get is the following

$$f(\mathbf{K}(\mathbf{K}') + \delta\mathbf{k}) = 1 + \mathrm{e}^{-\mathrm{i}(\mathbf{K}(\mathbf{K}')+\delta\mathbf{k})\cdot\mathbf{a}_1} + \mathrm{e}^{-\mathrm{i}(\mathbf{K}(\mathbf{K}')+\delta\mathbf{k})\cdot\mathbf{a}_2} \tag{2.44}$$

$$\simeq 1 + \left(-\frac{1}{2} + s\,\mathrm{i}\frac{\sqrt{3}}{2}\right)\left(1 - \mathrm{i}\delta\mathbf{k}\cdot\mathbf{a}_1\right) + \left(-\frac{1}{2} - s\,\mathrm{i}\frac{\sqrt{3}}{2}\right)\left(1 - \mathrm{i}\delta\mathbf{k}\cdot\mathbf{a}_2\right) \tag{2.45}$$

$$= \mathrm{i}\frac{1}{2}\delta\mathbf{k}\cdot(\mathbf{a}_1 + \mathbf{a}_2) + s\frac{\sqrt{3}}{2}\delta\mathbf{k}\cdot(\mathbf{a}_1 - \mathbf{a}_2) \tag{2.46}$$

$$= \frac{\sqrt{3}}{2}a(\mathrm{i}\delta k_x + s\delta k_y). \tag{2.47}$$

From Eq. (2.21) we know the expressions for the diagonal elements of the Hamiltonian matrix and using Eq. (2.47) we can write the Hamiltonian within the linear approximation as

$$\mathcal{H} = \begin{pmatrix} 0 & -t\frac{\sqrt{3}}{2}a(\mathrm{i}\delta k_x + s\delta k_y) \\ -t\frac{\sqrt{3}}{2}a(-\mathrm{i}\delta k_x + s\delta k_y) & 0 \end{pmatrix}. \tag{2.48}$$

We are interested in the eigenenergies of this effective Hamiltonian which we calculate as

$$\epsilon_{\delta\mathbf{k}\pm} = \pm|\mathcal{H}_{AB}| \tag{2.49}$$

$$= \pm\left(-t\frac{\sqrt{3}a}{2}\right)\sqrt{\delta k_x^2 + \delta k_y^2} \tag{2.50}$$

$$= \pm\left(-t\frac{\sqrt{3}a}{2}\right)|\delta\mathbf{k}|. \tag{2.51}$$

Having obtained an effective electron dispersion close to the Fermi energy we can also calculate the velocity of the electrons in the valence- and conduction bands within that approximation, given with the expression

$$\mathbf{v} = \frac{1}{\hbar}\frac{\partial\epsilon}{\partial(\delta\mathbf{k})} \tag{2.52}$$

$$= -\frac{\sqrt{3}ta}{2\hbar} = v_F, \tag{2.53}$$

where the last equal sign is justified by assumption that we are close to the Fermi energy. The remarkable fact about the expression in Eq. (2.53) is it's a constant, independent of wave vector $\delta\mathbf{k}$, with value $v_F \simeq c/300$. The final form of the dispersion relation within linear approximation is thus

$$\epsilon_{\delta\mathbf{k}\pm} = \pm\hbar v_F|\delta\mathbf{k}| \tag{2.54}$$

$$= \pm\hbar v_F\delta k. \tag{2.55}$$

The Hamiltonian in Eq. (2.48) is not an ordinary one but mimics a relativistic Hamiltonian and therefore the electrons within the linear approximation are better described with the Dirac equation rather than the usual Schrödinger equation. The reason is the crystal structure of graphene which we discussed in Section 1.4 where we found out that the hexagonal lattice consisted of two sublattices A and B. The linear dispersion relation in Eq. (2.55) implies that the electrons with wave vectors δk behave as if they were massless relativistic particles moving with constant velocity v_F. Due to this fact, these electrons are referred as Dirac electrons and the points $\mathbf{K}$ and $\mathbf{K}'$, where the conduction and valence bands cross, as Dirac points.

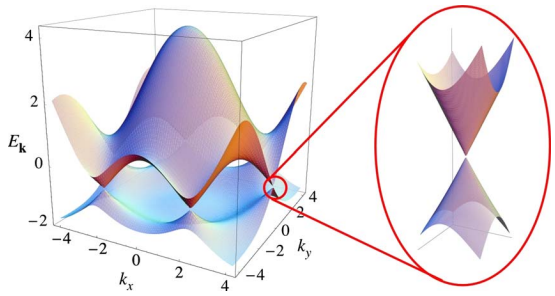

Figure 2.2: The dispersion relation and a zoom in to the linear part where the electrons move with constant velocity v_F.[18]

2.4 Hubbard interaction and triplet excitations

The latter term in the Hubbard Hamiltonian from Eq. (2.1) is the interaction term

$$\mathcal{H}_U = U \sum_{i\alpha} n_{i\alpha\uparrow} n_{i\alpha\downarrow}. \tag{2.56}$$

The sum is over all unit cells and both atoms within each unit cell. Physically what the term stands for is, it counts if there are two electrons occupying the same site with opposite spin. If that is the case, they get an energy penalty of U. Increasing energy in quantum mechanics indicates repulsion so the interaction term is a point like version of the classical Coulomb interaction between two charges having the same sign. It is point like in the sense it first acts when the two electrons occupy the same site. As we mentioned in the Introduction, Section 1.1 the goal of this project was to analyze if the Coulomb interaction generated formation of bound states in graphene. Triplet excitations from the ground state are a candidate to form bound states and to analyze that we have to construct these by rearranging the operators present in Eq. (2.56). Since electrons are fermions, the creation and annihilation operators of course obey the anti-commutation relations

$$\{c_i^\dagger, c_j^\dagger\} = 0, \quad \{c_i, c_j\} = 0, \quad \{c_i, c_j^\dagger\} = \delta_{i,j}. \tag{2.57}$$

Writing out the number operators in Eq. (2.56) and using the anti-commutator relations from Eq. (2.57) gives

$$\mathcal{H}_U = U \sum_{i\alpha} c^\dagger_{i\alpha\uparrow} c_{i\alpha\uparrow} c^\dagger_{i\alpha\downarrow} c_{i\alpha\downarrow} \tag{2.58}$$

$$= U \sum_{i\alpha} c^\dagger_{i\alpha\uparrow} c^\dagger_{i\alpha\downarrow} c_{i\alpha\downarrow} c_{i\alpha\uparrow} \tag{2.59}$$

$$= U \sum_{i\alpha} c^\dagger_{i\alpha\uparrow} (1 - c_{i\alpha\downarrow} c^\dagger_{i\alpha\downarrow}) c_{i\alpha\uparrow} \tag{2.60}$$

$$= U \sum_{i\alpha} \left(c^\dagger_{i\alpha\uparrow} c_{i\alpha\uparrow} - c^\dagger_{i\alpha\uparrow} c_{i\alpha\downarrow} c^\dagger_{i\alpha\downarrow} c_{i\alpha\uparrow} \right) \tag{2.61}$$

$$= U N_\uparrow - U \sum_{i\alpha} c^\dagger_{i\alpha\uparrow} c_{i\alpha\downarrow} c^\dagger_{i\alpha\downarrow} c_{i\alpha\uparrow}. \tag{2.62}$$

In the end we have an interaction operator consisting of two terms. First a constant term which is just the strength of interaction times the total number of electrons with spin up and then a negative term which contains a product of four second quantization operators. The former term we can safely neglect in our research because the correlation it describes will both be present in the excited state we will analyze and the ground state. At last we are interested in energy difference between those two states and therefore, in this context, it will vanish. What the latter term in Eq. (2.62) physically describes is (reading from the right) it annihilates an electron with spin up and then creates an electron with spin down which is the same as filling one hole with spin up. Altogether these two operators annihilate an electron–hole pair with total spin of 1. Continuing reading through the term, the third operator annihilates an electron with spin down, same as creating a hole with the opposite direction of spin en then at last it creates an electron with spin up. Again looking at what the two operators do combined, they create an electron–hole pair with total spin of 1. The reason for the opposite spin direction of electron and holes is that holes are inadequacies of electrons. For example when annihilating a spin up electron from the Fermi Sea containing equal numbers of spin up and spin down electrons results in one more spin down electrons than spin up electrons in total. This extra spin is contributed to the hole which therefore has an opposite spin to its electron.

What is to be noticed is that the electron and the hole in the same pair both are spin up, i.e. $|\uparrow_e\uparrow_h\rangle$, making the excitation in total have spin 1 because each participant has spin 1/2. The triplet excitation we therefore have generated has $m = 1$, which describes the projection of the angular momentum in the z-direction. We could have rearranged the operators in the original Hamiltonian from Eq. (2.56) in a different way, generating $\frac{1}{\sqrt{2}}(|\uparrow_e\downarrow_h\rangle + |\downarrow_e\uparrow_h\rangle)$, corresponding to $m = 0$ or $|\downarrow_e\downarrow_h\rangle$, having $m = -1$. These three triplet states all share the same energy in the absence of any external field so we can pick one of them, for example the $m = 1$ triplet to analyze more carefully in graphene.

What is also interesting to note in Eq. (2.58) to Eq. (2.62), is having before a repulsion due to an energy cost having to electrons occupying the same site we now have an attraction since there is a negative sign in front of the U denoting the strength of the Coulomb interaction. This can also be explained by another argument, namely now we are looking at interaction between electrons and holes where the electrons have negative charge but the holes have positive charge and therefore they attract each other, resulting in decreasing the total energy.

To write the interaction term in k-space we insert Eq. (2.39) to Eq. (2.62), allowing us to write

$$\begin{aligned}\mathcal{H}_U = -U \sum_{i\alpha} \Bigg[& \frac{1}{\sqrt{N}} \sum_{\mathbf{k}\beta_1} \mathrm{e}^{-\mathrm{i}\mathbf{k}\cdot\mathbf{R}_i} \, U_{\mathbf{k}\alpha\beta_1} c^\dagger_{\mathbf{k}\beta_1\uparrow} \\ & \frac{1}{\sqrt{N}} \sum_{\mathbf{k}'\beta_2} \mathrm{e}^{\mathrm{i}\mathbf{k}'\cdot\mathbf{R}_i} \, \left(U_{\mathbf{k}'\alpha\beta_2}\right)^* c_{\mathbf{k}'\beta_2\downarrow} \\ & \frac{1}{\sqrt{N}} \sum_{\mathbf{p}'\beta_3} \mathrm{e}^{-\mathrm{i}\mathbf{p}'\cdot\mathbf{R}_i} \, U_{\mathbf{p}'\alpha\beta_3} c^\dagger_{\mathbf{p}'\beta_3\downarrow} \\ & \frac{1}{\sqrt{N}} \sum_{\mathbf{p}\beta_4} \mathrm{e}^{\mathrm{i}\mathbf{p}\cdot\mathbf{R}_i} \, \left(U_{\mathbf{p}\alpha\beta_4}\right)^* c_{\mathbf{p}\beta_4\uparrow} \Bigg]. \end{aligned} \tag{2.63}$$

Where each Fourier transform is written with its own momentum and β index. Grouping appropriated terms together and performing the sum over α results in

$$\begin{aligned}\mathcal{H}_U = -\frac{U}{N^2} \sum_i \sum_{\substack{\mathbf{k}\mathbf{k}' \\ \mathbf{p}\mathbf{p}'}} \sum_{\substack{\beta_1\beta_2 \\ \beta_3\beta_4}} & \mathrm{e}^{\mathrm{i}\left(\mathbf{k}'-\mathbf{k}+\mathbf{p}-\mathbf{p}'\right)\cdot\mathbf{R}_i} \\ & \Big[U_{\mathbf{k}A\beta_1} \left(U_{\mathbf{k}'A\beta_2}\right)^* U_{\mathbf{p}'A\beta_3} \left(U_{\mathbf{p}A\beta_4}\right)^* \\ & \quad + U_{\mathbf{k}B\beta_1} \left(U_{\mathbf{k}'B\beta_2}\right)^* U_{\mathbf{p}'B\beta_3} \left(U_{\mathbf{p}B\beta_4}\right)^* \Big] \\ & c^\dagger_{\mathbf{k}\beta_1\uparrow} c_{\mathbf{k}'\beta_2\downarrow} c^\dagger_{\mathbf{p}'\beta_3\downarrow} c_{\mathbf{p}\beta_4\uparrow}. \end{aligned} \tag{2.64}$$

The sum over unit cells i, can now be performed since it only appears in the exponential function. It produces a momentum conservation constraint since $\sum_i \mathrm{e}^{\mathrm{i}\hat{q}\cdot\mathbf{R}_i} = N\delta_{\hat{\mathbf{q}},\mathbf{K}}$ where $\mathbf{K}$ is a reciprocal lattice vector and we have called $\hat{\mathbf{q}} = \mathbf{k}' - \mathbf{k} + \mathbf{p} - \mathbf{p}'$. The δ-function therefore gives

$$\mathbf{k}' - \mathbf{k} + \mathbf{p} - \mathbf{p}' = \mathbf{K} \tag{2.65}$$

This constraint can be satisfied by changing from $\mathbf{k}'$ and $\mathbf{p}'$ to a new variable $\mathbf{q}$

defined as

$$\mathbf{q} \equiv \mathbf{k} - \mathbf{k}', \tag{2.66}$$

$$\Rightarrow \quad \mathbf{p} - \mathbf{p}' = \mathbf{q} + \mathbf{K}. \tag{2.67}$$

Throughout this thesis we take $\mathbf{K} = \mathbf{0}$, which is also a reciprocal lattice vector corresponding to $m_1 = m_2 = 0$ from Eq. (1.19). This is the same as neglecting Umklapp scattering which is a scattering process where the sum of the incoming momenta lies outside the first Brillouin zone. Consequently the wave vectors for $\mathbf{k}'$ and $\mathbf{p}'$ are written as

$$\mathbf{k}' = \mathbf{k} - \mathbf{q}, \tag{2.68}$$

$$\mathbf{p}' = \mathbf{p} - \mathbf{q}. \tag{2.69}$$

Inerting these two equations into Eq. (2.64) after having performed the sum over i results in

$$\begin{aligned}\mathcal{H}_U = -\frac{U}{N} \sum_{\mathbf{kpq}} \sum_{\substack{\beta_1\beta_2 \\ \beta_3\beta_4}} \Big[& U_{\mathbf{k}A\beta_1} \left(U_{\mathbf{k}-\mathbf{q}A\beta_2}\right)^* U_{\mathbf{p}-\mathbf{q}A\beta_3} \left(U_{\mathbf{p}A\beta_4}\right)^* \\ & + U_{\mathbf{k}B\beta_1} \left(U_{\mathbf{k}-\mathbf{q}B\beta_2}\right)^* U_{\mathbf{p}-\mathbf{q}B\beta_3} \left(U_{\mathbf{p}B\beta_4}\right)^* \Big] \\ & \times c^\dagger_{\mathbf{k}\beta_1\uparrow} c_{\mathbf{k}-\mathbf{q}\beta_2\downarrow} c^\dagger_{\mathbf{p}-\mathbf{q}\beta_3\downarrow} c_{\mathbf{p}\beta_4\uparrow}.\end{aligned} \tag{2.70}$$

This is how the interaction part of the Hamiltonian looks after having transformed it from real space in Eq. (2.56) to k-space with help of Eq. (2.39). In Fig. 2.3 there are schematic drawings of what the Hamiltonian in Eq. (2.70) could render when an electron–hole pair is annihilated close to one Dirac point and another is created. On the figure the dispersion relation is drawn according to Eq. (2.55) even though later in this thesis we will use the whole dispersion to calculate the dynamics of these electron–hole pairs. The filled circles denote electrons, the open circles denote holes and the arrows drawn on top of them indicate the spin direction. The chemical potential is μ and we should imagine everything below it filled with electrons except the two open circles. At last the arrows between the electrons and holes stands for annihilation (arrowtail) and creation (arrowhead) of a particle.

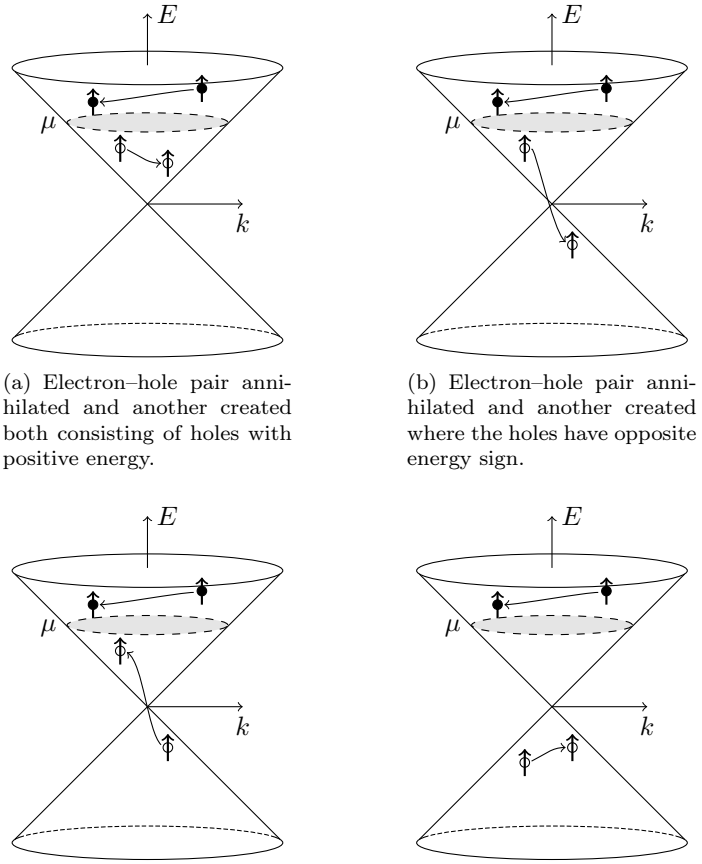

(a) Electron–hole pair annihilated and another created both consisting of holes with positive energy.

(b) Electron–hole pair annihilated and another created where the holes have opposite energy sign.

(c) Electron–hole pair annihilated and another created where the holes have opposite energy sign.

(d) Electron–hole pair annihilated and another created both consisting of holes with negative energy.

Figure 2.3: Schematic drawings of what the interacting Hamiltonian in Eq. (2.70) could render. In all cases an electron–hole pair with spin 1 is annihilated and another electron–hole pair with the same total spin is created. The processes are drawn within the linear approximation of the dispersion relation so the crossing point between the conduction and valence bands could either be K or K'.

In Fig. 2.4 we show two possible outcomes of the interacting Hamiltonian could produce where one electron–hole pair is annihilated close to one Dirac point and another created close to the other Dirac point.

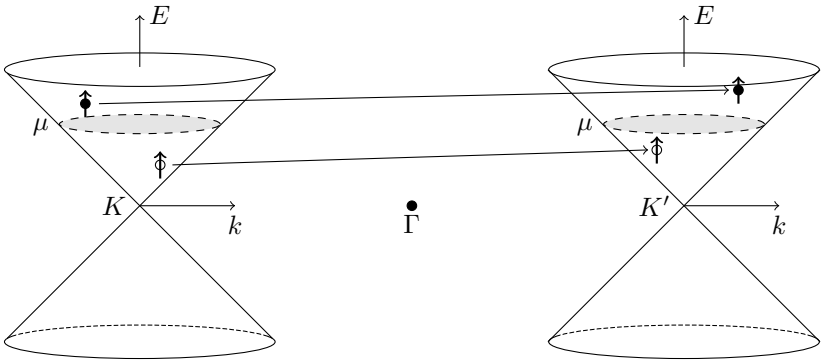

(a) An electron–hole pair annihilated close to K and created close to K'.

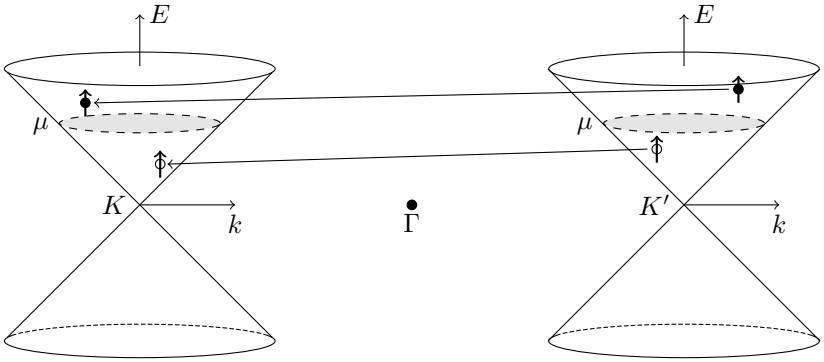

(b) An electron–hole pair annihilated close to K' and created close to K.

Figure 2.4: More schematic drawings of what the interacting Hamiltonian in Eq. (2.70) could render. In these two cases an electron–hole pair is annihilated close to $K(K')$ point and created close to the $K'(K)$. Both processes have the same properties as the one in Fig. 2.3(a) where all participants have positive energy. This could of course also be drawn for the other figures in Fig. 2.3.

Having the Hamiltonian written in k-space allows us to let it act on appropriated states generating interesting results which is what we will take look at in the upcoming chapter.

Chapter 3

Triplet excitations in graphene

As the title of this chapter states, we are going to investigate the properties of triplet excitations in graphene. First we derive the spectrum of these excitations and in the second section we show how our Hamiltonian works in the subspace containing the triplet excitations.

3.1 Electron–hole excitation spectrum

Having seen in Eq. (2.70) of Section 2.4 that the interaction operator first annihilates an electron–hole pair and then creates another, it would be interesting to know the spectrum of these electron–hole excitations. We therefore want to determine for which wave vectors q and energies $\hbar\omega$ they can be generated. The tool needed to decide that is the density of states

$$\rho(\mathbf{q},\omega) = \sum_{\mathbf{k}} \delta\left(\hbar\omega - \epsilon_{\mathbf{k}} + \epsilon_{\mathbf{k}-\mathbf{q}}\right). \tag{3.1}$$

To be able to get nice, analytical expression for the electron–hole excitation spectrum we use the linear approximation for the electron dispersion from Eq. (2.55). What Eq. (3.1) then describes is the density of these excitations in k-space for a given wave vector $\mathbf{q}$. The sum is over all wave vectors $\mathbf{k}$ within the linear approximation and each time an electron–hole pair with energy $\epsilon_{\mathbf{k}} - \epsilon_{\mathbf{k}-\mathbf{q}}$, where the electron has energy $\epsilon_{\mathbf{k}}$ and the hole has energy $\epsilon_{\mathbf{k}-\mathbf{q}}$, equals ω i.e. $\omega = \epsilon_{\mathbf{k}} - \epsilon_{\mathbf{k}-\mathbf{q}}$ the δ-function gives a non-zero contribution to the density of states.

In Section 2.2 we found out that pristine graphene has a filled valence band and an empty conduction band and therefore Fermi energy, $E_F = 0$. That was due to the hexagonal lattice structure of graphene containing two carbon atoms in each unit cell. What can be done with experimental techniques, that

we won't describe in this report, is to manipulate the Fermi energy by adding or subtracting electrons and therefore tuning the Fermi energy away from zero. This procedure is called doping, where the material can either be doped with electrons and thereby increasing the Fermi energy or be doped by holes resulting in the opposite change in Fermi energy. Let's consider electron doped graphene which implies that holes can be created both with negative and positive energy i.e. both within the valence and conduction band. The electrons can of course only be excited above the Fermi surface and therefore can only have positive energy. First we look at electron–hole pairs where the hole has negative energy, that kind of excitation is called an interband excitation due to the electron and hole exists in different bands.

i) Interband excitations
In this case we have that $\epsilon_{\mathbf{k}} > \mu$, where μ is the chemical potential describing the value of doping, and $\epsilon_{\mathbf{k}-\mathbf{q}} < 0$. From the δ-function in Eq. (3.1) we get

$$\hbar\omega = \epsilon_{\mathbf{k}} - \epsilon_{\mathbf{k}-\mathbf{q}}. \tag{3.2}$$

Inserting the linearized dispersion relation gives

$$\omega = v_F \left(|\mathbf{k}|+|\mathbf{k}-\mathbf{q}|\right) \tag{3.3}$$
$$= v_F \left(k + \sqrt{k^2+q^2-2kq\cos\theta}\right). \tag{3.4}$$

Collecting the terms on one side we end up with a quadratic equation in ω

$$\omega^2 - 2v_F k\omega - (v_F q)^2 + 2v_F^2 kq\cos\theta = 0, \tag{3.5}$$

with solutions

$$\omega = v_F \left(k \pm \sqrt{k^2+q^2-2kq\cos\theta}\right). \tag{3.6}$$

Obviously ω takes a maximum value when the the positive solution is used and $\cos\theta = -1$, giving

$$\omega(k, \cos\theta = -1) \equiv \omega_{max} = v_F \left(k + \sqrt{k^2+q^2+2kq}\right) \tag{3.7}$$
$$= v_F \left(k + |k+q|\right) \tag{3.8}$$
$$= v_F(2k+q). \tag{3.9}$$

The minimum value of ω is gotten from the negative solution and when

$\cos\theta = 1$, which results in

$$\omega(k, \cos\theta = 1) \equiv \omega_{min} = v_F \left(k + \sqrt{k^2 + q^2 - 2kq}\right) \tag{3.10}$$

$$= v_F \left(k - |k - q|\right) \tag{3.11}$$

$$= \begin{cases} v_F(k - (k - q)), & k > q \\ v_F(k - (q - k)), & k < q \end{cases} \tag{3.12}$$

$$= \begin{cases} v_F q, & k > q \\ v_F(-q + 2k), & k < q \end{cases}. \tag{3.13}$$

What defines the region in (q, ω)-space is the electron is constrained to

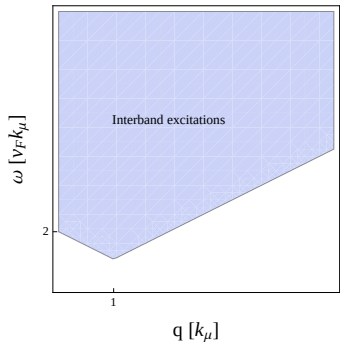

(a) Region of (q, ω)-space consisting of interband excitations.

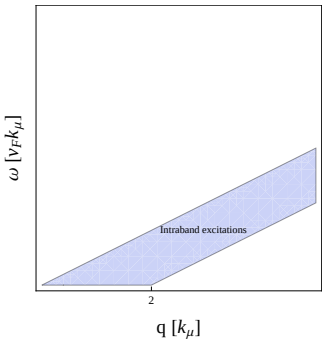

(b) Region of (q, ω)-space consisting of interwband excitations.

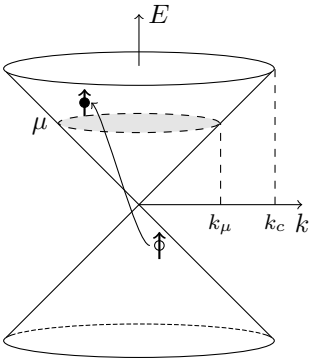

(c) Interband excitation.

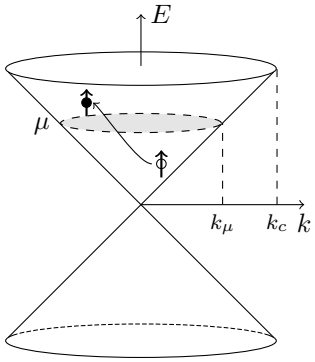

(d) Intraband excitation.

Figure 3.1: Plots showing the excitations spectrum generated from two different processes i.e. an electron–hole excitation consists of an electron with positive energy and a hole with either negative (a),c)) or positive (b),d)) energy.

have magnitude of the wave vector k so $k_\mu < k < k_c$ where k_μ is the magnitude of wave vector corresponding the chemical potential and k_c is the

magnitude of the vector corresponding to some cut-off where linearization of the dispersion relation is no longer valid. A plot of this region can be seen in Fig. 3.1(a) and of this kind of excitation in Fig. 3.1(c).

ii) Intraband excitations

By redefining the wave vectors of the electron and the hole so $\mathbf{k}' = \mathbf{k} - \mathbf{q}$ is the wave vector of the hole implying that $\mathbf{k} = \mathbf{k}' + \mathbf{q}$ is the wave vector of the electron we can do a similar calculation as in case i). The δ-function gives

$$\hbar\omega = \epsilon_{\mathbf{k}'+\mathbf{q}} - \epsilon_{\mathbf{k}'}. \tag{3.14}$$

Again inserting the linearized dispersion relation as in Eq. (3.15) we obtain, now with a minus sign between the two terms,

$$\omega = v_F \left(|\mathbf{k}' + \mathbf{q}| - |\mathbf{k}'|\right) \tag{3.15}$$

$$= v_F \left(\sqrt{k'^2 + q^2 - 2k'q\cos\theta} - k'\right). \tag{3.16}$$

Collecting the terms on one side we end up with a quadratic equation in ω

$$\omega^2 + 2v_F k'\omega - (v_F q)^2 - 2v_F^2 k' q\cos\theta = 0 \tag{3.17}$$

with solutions

$$\omega = v_F \left(-k' \pm \sqrt{k'^2 + q^2 + 2k'q\cos\theta}\right) \tag{3.18}$$

In this case ω takes a maximum value when the the positive solution is used and $\cos\theta = 1$ giving

$$\omega(k, \cos\theta = 1) \equiv \omega_{max} = v_F \left(-k + \sqrt{k'^2 + q^2 + 2'kq}\right) \tag{3.19}$$

$$= v_F \left(-k + |k + q|\right) \tag{3.20}$$

$$= v_F q. \tag{3.21}$$

The minimum value of ω is gotten from the negative solution and when $\cos\theta = -1$

$$\omega(k, \cos\theta = -1) \equiv \omega_{min} = v_F \left(-k' - \sqrt{k'^2 + q^2 - 2k'q}\right) \tag{3.22}$$

$$= v_F \left(-k' - |k' - q|\right) \tag{3.23}$$

$$= \begin{cases} v_F(-k' - (k' - q)), & k' > q \\ v_F(-k' - (q - k')), & k' < q \end{cases} \tag{3.24}$$

$$= \begin{cases} v_F(q - 2k'), & k' > q \\ -v_F q, & k' < q \end{cases}. \tag{3.25}$$

The region confined in (q, ω)-space due this kind of excitations is constrained by the magnitude of the hole wave vectors which has to fulfill $0 < k' < k_\mu$. A plot of this region can be seen in Fig. 3.1(b) and in Fig. 3.1(d) there is an example of an intraband excitation. In the case of no doping it is interesting to see how the excitation spectrum looks and also how it varies when doping is increased from zero to some arbitrary value. That is what can be seen in Fig. 3.2 where in the case of zero doping no window is present in the excitation spectrum and it mimics the linearized dispersion relation. Increasing the doping opens a window in the spectrum and in the case of high doping the excitation spectrum resembles the one for two-dimensional electron gas. That is easy to understand since for high energies the dispersion relation is quadratic which is evident from Fig. 2.1, having contours that are circular inside the first Brillouin Zone.

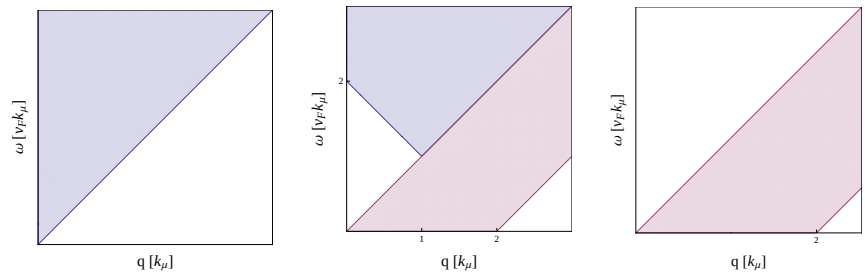

(a) No doping and the spectrum mimics the liner dispersion relation.

(b) Moderate value of doping and a window is opened in the excitation spectrum.

(c) High value of doping and the spectrum looks more like the one for 2DEG we saw in Fig. (1.8(b)).

Figure 3.2: The figures show the electron–hole excitation spectrum for three different values of doping μ.

The very important thing about the (q, ω) spectrum has to do with the lifetime of the excitations, or the so called damping mechanism. It turns out that the density of states Eq. (3.1) is proportional to the decay time of these excitations i.e. $\rho \propto \tau$. That implies, when the density of states is zero, for example in the window of doped graphene, the lifetime of the modes present there is infinite, indicating a bound state solution in the material. Whereas the modes within the allowed regions acquire finite lifetime and decay.

Having found the electron–hole excitation spectrum without interaction we are in stand to see how this picture is modified by taking the interactions into account.

3.2 Subspace of triplet excitations

In this thesis we will consider a virtual graphene crystal containing 3200 protons and 3200 electrons where each particle interacts with all the others, either by repulsion or attraction, due do Coulomb's law. The interaction strength depends on the spatial coordinates of every particle at a given time and in a quantum mechanical system described by a wave function we therefore have to solve the Schrödinger equation in 3×3200 dimensions to understand the behavior of the electrons. That is very hard and in larger systems it becomes impossible. What we can do is to recognize that the many-body system has a ground state along with infinite series of excited states with increasing energy. Often we are only interested in the lowest lying excited states close to the ground state because at low temperatures these are most releavant. We would like to examine the energies for triplet excitations from the ground state consisting of the filled Fermi Sea, so we enhance the total electron spin by unity. We therefore look at a subspace of the total many-body Hilbert space which consists only of these excitations. The states living in that subspace can all be written as

$$|\psi_{\mathbf{q}}\rangle = \sum_{\mathbf{k}'\beta\beta'} a_{\mathbf{k}'\beta\beta'} c^\dagger_{\mathbf{k}'\beta\uparrow} c_{\mathbf{k}-\mathbf{q}\beta'\downarrow} |FS\rangle, \tag{3.26}$$

which is the filled Fermi Sea with linear combination of triplet electron–hole pairs. The coefficients $a_{\mathbf{k}\beta\beta'}$ are in general complex numbers. In Section 3.1 we argumented for that an electron can only be excited above the chemical potential which in electron doped graphene has positive energy so β, the energy index of the electrons, must be $+$ where as the energy index for the holes β' can either be $+$ or $-$. We would like to solve the Schrödinger equation for a given wave vector $\mathbf{q}$

$$\mathcal{H}|\psi_{\mathbf{q}}\rangle = E_{\mathbf{q}}|\psi_{\mathbf{q}}\rangle, \tag{3.27}$$

where the full Hamiltonian is

$$\mathcal{H} = \mathcal{H}_{TB} + \mathcal{H}_U \tag{3.28}$$

$$= \sum_{\mathbf{k}\beta\sigma} \epsilon_{\mathbf{k}\beta} c^\dagger_{\mathbf{k}\beta\sigma} c_{\mathbf{k}\beta\sigma} - \frac{U}{N} \sum_{\mathbf{kp}} \sum_{\beta_2\beta_3} \Big[U_{\mathbf{k}A+} \left(U_{\mathbf{k}-\mathbf{q}A\beta_2}\right)^* U_{\mathbf{p}-\mathbf{q}A\beta_3} \left(U_{\mathbf{p}A+}\right)^* + U_{\mathbf{k}B+} \left(U_{\mathbf{k}-\mathbf{q}B\beta_2}\right)^* U_{\mathbf{p}-\mathbf{q}B\beta_3} \left(U_{\mathbf{p}B+}\right)^* \Big] c^\dagger_{\mathbf{k}+\uparrow} c_{\mathbf{k}-\mathbf{q}\beta_2\downarrow} c^\dagger_{\mathbf{p}-\mathbf{q}\beta_3\downarrow} c_{\mathbf{p}+\uparrow}. \tag{3.29}$$

Now letting this Hamiltonian work on the state given in Eq. (3.26) results in

$$\mathcal{H}|\psi_{\mathbf{q}}\rangle = \sum_{\mathbf{k}\beta'} a_{\mathbf{k}+\beta'} \left(E_0 + \epsilon_{\mathbf{k}} - \epsilon_{\mathbf{k}-\mathbf{q}}\right) c^\dagger_{\mathbf{k}+\uparrow} c_{\mathbf{k}-\mathbf{q}\beta'\downarrow} |FS\rangle + \sum_{\mathbf{k}\mathbf{k}'} \sum_{\beta_2\beta'} a_{\mathbf{k}'+\beta'} \mathrm{U}^{\mathbf{k}}_{\mathbf{k}'}(\mathbf{q})_{\beta_2\beta'} c^\dagger_{\mathbf{k}+\uparrow} c_{\mathbf{k}-\mathbf{q}\beta_2\downarrow} |FS\rangle \tag{3.30}$$

$$= E_{\mathbf{q}} \sum_{\mathbf{k}'\beta'} a_{\mathbf{k}'+\beta'} c^\dagger_{\mathbf{k}'+\uparrow} c_{\mathbf{k}'-\mathbf{q}\beta'\downarrow} |FS\rangle. \tag{3.31}$$

To explain how Eq. (3.30) came about we look carefully at each term. The former one is what the diagonal tight-binding term generates, it gives the energy of the filled Fermi Sea, E_0, plus the energy of the electron minus the energy of the hole i.e. the ground state energy plus the excitation energy. The latter term is what the interaction term generates, for getting non-zero outcome $\mathbf{p} = \mathbf{k}'$ and $\beta_3 = \beta'$ so what the interaction does, as described before, it annihilates an electron pair with momentum $\mathbf{k}'$ and generate another with momentum $\mathbf{k}$. The probability amplitude for that given process is $\mathrm{U}^{\mathbf{k}}_{\mathbf{k}'}(\mathbf{q})_{\beta_2\beta'}$, which stores all the matrix elements involved

$$-\frac{U}{N}\Big[U_{\mathbf{k}A+}\left(U_{\mathbf{k}-\mathbf{q}A\beta_2}\right)^* U_{\mathbf{k}'-\mathbf{q}A\beta'}\left(U_{\mathbf{k}'A+}\right)^* \tag{3.32}$$

$$+ U_{\mathbf{k}B+}\left(U_{\mathbf{k}-\mathbf{q}B\beta_2}\right)^* U_{\mathbf{k}'-\mathbf{q}B\beta'}\left(U_{\mathbf{k}'B+}\right)^*\Big] \equiv \mathrm{U}^{\mathbf{k}}_{\mathbf{k}'}(\mathbf{q})_{\beta_2\beta'} \tag{3.33}$$

Eq. (3.31) can be written in a matrix format, making the physics it describes more visible

$$\begin{pmatrix} \epsilon_{\mathbf{k}_1} - \epsilon_{\mathbf{k}_1-\mathbf{q}} & U^{\mathbf{k}_1}_{\mathbf{k}_2}(\mathbf{q})_{\beta_2\beta'} & \cdots & U^{\mathbf{k}_1}_{\mathbf{k}_N}(\mathbf{q})_{\beta_2\beta'} \\ U^{\mathbf{k}_2}_{\mathbf{k}_1}(\mathbf{q})_{\beta_2\beta'} & \ddots & & \vdots \\ \vdots & & \ddots & \\ U^{\mathbf{k}_N}_{\mathbf{k}_1}(\mathbf{q})_{\beta_2\beta'} & \cdots & & \epsilon_{\mathbf{k}_N} - \epsilon_{\mathbf{k}_N-\mathbf{q}} \end{pmatrix} \begin{pmatrix} a_{\mathbf{k}_1} \\ \\ \vdots \\ \\ a_{\mathbf{k}_N} \end{pmatrix} = (E_{\mathbf{q}} - E_0) \begin{pmatrix} a_{\mathbf{k}_1} \\ \\ \vdots \\ \\ a_{\mathbf{k}_N} \end{pmatrix}. \tag{3.34}$$

The Hamiltonian matrix which is $N \times N$ dimensional consists of the tight-binding diagonal elements and the non-diagonal elements coming from the interaction Hamiltonian. By solving Eq. (3.34) we can find the eigenvectors and the eigenvalues $\hbar\omega_{\mathbf{q}} = E_{\mathbf{q}} - E_0$ which are the triplet excitations energies. In the next chapter we will solve this problem with the help of numerical computation.

Chapter 4

Numerical investigation

To solve the Hamiltonian for our system we use numerical methods described in this chapter. We show how the Coulomb interaction generate formation of bound states in graphene and analyze one of those for a given value of interaction strength.

4.1 Change of units

Before diving into the numerical investigation on the triplet excitations in graphene, we would like to explain and derive how the variables we will see on different figures and plots in Section 4.2 were made dimensionless. That was done by measuring all energies in t's, the hopping energy of the Hubbard Hamiltonian in Eq. (2.1), which is approximately $-2.8\,\text{eV}$ [18]. Dimensionless variables we will denote with a tilde above the symbols. The Hubbard interaction parameter U and the chemical potential μ in this language therefore become

$$\tilde{U} = \frac{U}{|t|} \tag{4.1}$$

$$\text{and} \qquad \tilde{\mu} = \frac{\mu}{|t|}. \tag{4.2}$$

We play the same game with the linear dispersion relation Eq. (2.55)

$$\tilde{\epsilon}_{\mathbf{k}\pm} = \frac{\epsilon_{\mathbf{k}\pm}}{|t|} = \pm\frac{\hbar v_F |\mathbf{k}|}{|t|}. \tag{4.3}$$

Multiplying with $1 = {}^{a}/_{a}$ and inserting the expression for the Fermi velocity Eq. (2.53) we get

$$\tilde{\epsilon}_{\mathbf{k}\pm} = \pm\frac{\hbar v_F a k}{|t|a} \tag{4.4}$$

$$= \pm\frac{\hbar\left(-\frac{\sqrt{3}ta}{2\hbar}\right)ak}{|t|a} \tag{4.5}$$

$$= \pm\frac{\sqrt{3}}{2}ak. \tag{4.6}$$

where we have defined $|\mathbf{k}| \equiv k$. At last we insert for the lattice constant $a = \sqrt{3}a_{c-c}$ to get

$$\tilde{\epsilon}_{\mathbf{k}\pm} = \pm\frac{3}{2}a_{c-c}k \tag{4.7}$$

$$= \pm\tilde{v}_F\tilde{k}. \tag{4.8}$$

Where we have defined two new dimensionless variables

$$\tilde{v}_F \equiv \frac{3}{2}, \tag{4.9}$$

$$\tilde{k} \equiv a_{c-c}k. \tag{4.10}$$

Another variable we will see a number of times in Section 4.2 is $\tilde{\omega}$, a dimensionless version of the excitation energy, defined as

$$\tilde{\omega} \equiv \frac{\hbar\omega}{|t|}. \tag{4.11}$$

Eq. (4.11) is justified by writing the energy $\epsilon_{\mathbf{k}\pm}$ as $\epsilon_{\mathbf{k}\pm} = \pm\hbar\omega$ and divide by $|t|$.

4.2 Numerical calculation

In Section 3.2 we derived a matrix equation determining the eigenenergies corresponding to triplet excitations from the ground state of graphene. That we did by letting the Hamiltonian we had prepared in Chapter 2 work on an state which is the filled Fermi Sea with linear combination of triplet electron–hole excitations, Eq. (3.26). All in all ending up with Eq. (3.34) waiting to be solved. To avoid any unnecessary uncertainties, we want solve this problem exact i.e using the full dispersion relation from Eq. (2.25) rather than making approximations like using the linearized version of it. In reality the dispersion relation for graphene is the one given in Eq. (2.25) so why not to use it if possible? The dimension of the matrix equation to be solved is $N \times N$ where N is the number of allowed k-states from Eq. (2.13). Obviously this will be to much of a task to do with hand power so we let the computers do the work through the program

Mathematica. The code used can be seen in Appendix A.

We discretized the reciprocal unit cell, spanned by the two reciprocal lattice vectors $\mathbf{b}_1$ and $\mathbf{b}_2$ seen in Fig. 2.1, in 1600 allowed k-states representing a piece of graphene consisting of equal amount unit cells. In Fig. 4.1 we see the discretization of the unit cell where the red dots representes allowed k-states obtained with boundary conditions from Eq. (2.10). We saw in Section 1.4 that each reciprocal unit cell contains the whole range of possible wave vectors so no information should be lost with our choice.

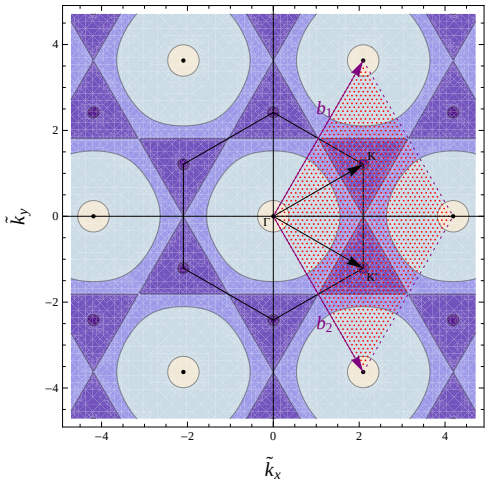

Figure 4.1: Reciprocal space and the discretized unit cell. The red dots represent allowed k-states.

In Section 3.1 we found out when doping graphene with electrons a window in the (q, ω)-spectrum appeared. A place where the triplet excitations will not be damped. In our numerical calculations we therefore set $\tilde{\mu} = 0.2$ so this window will be present. That corresponds to adding $\simeq 213$ electrons to the material according to the formula

$$\frac{\tilde{\mu}}{\Delta\tilde{E}_c}\, 2N = \frac{0.2}{3}\, 2 \cdot 1600 \simeq 213, \tag{4.12}$$

where $\Delta\tilde{E}$ is the band width of the conduction band and N the number of unit cells. This means then that $\simeq 213$ sites will be double occupied with two electrons having opposite spin. Raising the chemical potential decreases the area electrons in the electron–hole pairs can live on, since they have to be above the Fermi Sea having wave vectors $k > k_\mu$. In Fig. 4.2 we see again the discretized unit cell in reciprocal space but with $\tilde{\mu} = 0.2$ explaining the inadequacy of allowed electron k-states around the Dirac points. The next important step in the numerical calculation is to classify the two different excitation processes,

interband and intraband excitations. As we saw in Eq. (3.26) a triplet excitation is generated by annihilating an electron below the chemical potential with wave vector $\mathbf{k}-\mathbf{q}$ and create another one above the chemical potential with wave vector $\mathbf{k}$. In the program we therefore set the wave vector $\mathbf{q}$ to a given value and for all the allowed $\mathbf{k}$ vectors we calculate $\mathbf{k}-\mathbf{q}$. If $|\mathbf{k}-\mathbf{q}|< k_\mu$, then we have an intraband excitation whereas for all $|\mathbf{k}-\mathbf{q}|> 0$ we have an interband excitation, since the valence band is just the mirror image of the conduction band. In Fig. 3.1(c) and Fig. 3.1(d) we showed illustrations of these processes. Obviously the interband excitations will be much more frequent than the intraband excitations since the energy range from 0 to $\tilde{\mu}$ is much smaller than $\Delta\tilde{E}_v$ the band width of the valence band.

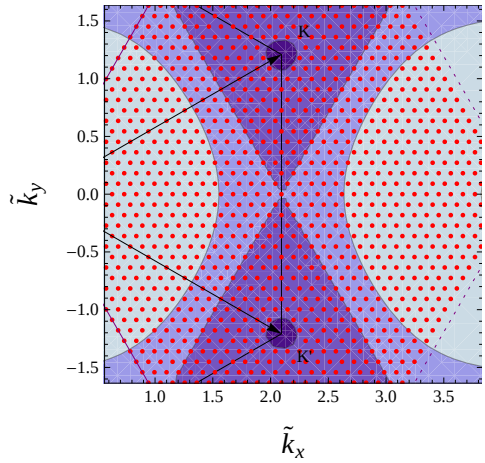

Figure 4.2: Reciprocal space and the discretized unit cell with nonzero chemical potential. The red dots represent allowed k-states.

Now we let Mathematica work out all the $2.56 \cdot 10^6$ matrix elements of the 1600×1600 matrix in Eq. (3.34). At last we ask for the eigenvalues of this matrix but before we show and discuss the outcomes of these evaluations we would like to address the reason for the choice of $\tilde{\mu}$ and N. These two numbers have to be somehow linked since $\tilde{\mu}$ determines the size of the window in the $(\tilde{q}, \tilde{\omega})$-spectrum and N sets the concentration of allowed k-states. So in the case of low N and low $\tilde{\mu}$ the window becomes "invisible" and we won't be able to obtain any interesting physics inside it. Another extreme case would be to set N to a very large number, approaching the continuous limit which would not require large $\tilde{\mu}$ since the k-states would be very dense, but then the size of the matrix equation would explode and no computer would be able to solve that. Thus it is a compromise between few factors, to do an calculation on an enough large sample that captures the important physics and to stick within the range of reasonably long computer times. We chose as said before $N = 1600$ and $\tilde{\mu} = 0.2$ which manages to fulfill the criteria mentioned above since a graphene flake containing 3200 carbon atoms for sure should reminiscence a realistic graphene

crystal and a project like this is finished within set time range.

For $\tilde{\mu} = 0.2$ the window is between $\tilde{q} = 0$ and $\tilde{q} = \tilde{\mu}/\tilde{v}_F \simeq 0.13$ so in the search for excitations in the window we choose $\tilde{q}$'s within this interval. The strength of the Coulomb interaction is controlled by the Hubbard U and is not a well-defined parameter in graphene. In Fig. 4.3 we have plotted the eigenvalues of the matrix equation in Eq. (3.34) for eleven different values of $\tilde{U} = \{0.0, 1.0, 2.0, 3.0, 3.2, 3.4, 3.6, 3.8, 4.0, 4.2, 4.4\}$ and $\tilde{q} = \{0.02, 0.04, 0.06, 0.08, 0.10\}$, these are showed with red disks. For comparison we have also plotted as blue disks the eigenvalues for the noninteracting case which can be found on the diagonal line in Eq. (3.34). For $\tilde{U} = 0$ the red and the blue disks are of course centered at the same point, obvious from Fig. 4.3(a). As the strength of the interaction is increased the eigenvalues shift to lower energies. That is due to the minus sign in the Hamiltonian Eq. (2.70), so it is a property of the triplet excitations we are investigating. In Section 3.1 we derived electron–hole excitation spectrum neglecting the interaction. These regions where the density of states is nonzero is of course a theoretical considerations in limit of $N \to \infty$, where the k-states would be infinite dense as well. That is of course not the case for the virtual graphene crystal we are investigating with $N = 1600$. So what we get are discrete eigenvalues not filling the whole regions of interband and intraband excitations. We can for example count the number of intraband excitations for the $\tilde{q}$'s we have evaluated for, there are in total eight excitations, one for $\tilde{q} = 0.04$, two for $\tilde{q} = 0.06$ and $\tilde{q} = 0.8$ and three for $\tilde{q} = 0.10$.

One excitation for each $\tilde{q}$ evaluated can be found exactly at the boundaries between the window and the intraband, whereas for the interband excitations there is a gap between the lowest lying eigenvalue for each $\tilde{q}$ and the theoretical boundary between the window and the band. The reason for this is just that the discretization in k-space for $N = 1600$ results in for a given $\mathbf{q}$ that $\epsilon_{\mathbf{k}} - \epsilon_{\mathbf{k}-\mathbf{q}}$ does not give any values closer to the boundary. Increasing N would immediately change this as mentioned before. We see in Figs. 4.3(a) - (c) where $\tilde{U} = 0, 1, 2$ almost no difference in red and blue disks indicating that the kinetic term in the Hamiltonian still dominates the dynamics and interaction between the electrons does not have any impact. In Figs. 4.3(d) - (f) we begin to see effects due to the interaction, where the lowest lying eigenvalues are becoming more and more isolated from the continuum. One could say for this piece of graphene under considerations, they were living in the window of the electron–hole excitation spectrum but they are still within the theoretical continuum of damped electron-hole pairs. In conjugated polymers wich are molecular systems of connected p-orbitals where the electrons are considered delocalized just as we described for graphene in Section 1.4.1, the Coulomb interaction is $\sim 10\,\text{eV}$ or $\sim 3.6t$ [19] and for graphene the strength is also believed to be in this range [20]. Figs. 4.3(g) - (i) are all approximately on this interval and there we see a rather clear dispersion relation of long living triplet excitations. Of course the dispersion relation is a continuous mode even though it is showed as discrete points on the figures, letting the program solve for more closely spaced $\tilde{q}$-values would

yield that. In Figs. 4.3(j) - (k) we are probably reaching an upper limit for the interaction strength but as we can see the dispersion relation is well isolated from the continuum. In Table 4.1 we have converted the values of the interaction strength to electron volts by using $|t| = 2.8\,\text{eV}$ in Eq. (4.1).

$\tilde{U}$	0	1	2	3	3.2	3.4	3.6	3.8	4.0	4.2	4.4
U [eV]	0	2.8	5.6	8.4	9.0	9.5	10.1	10.6	11.2	11.8	12.3

Table 4.1: Table showing the values of the Coulomb interaction strength according to Eq. (4.1).

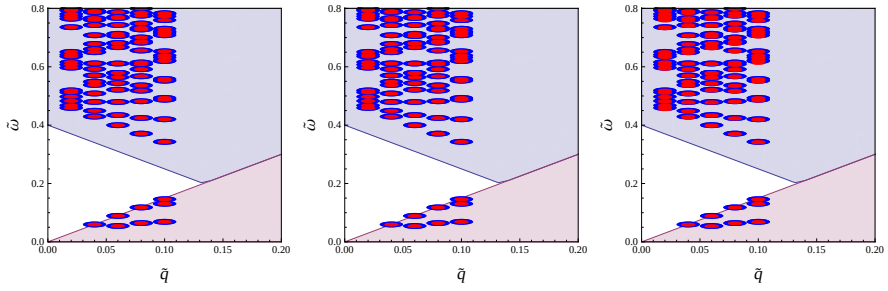

(a) $\tilde{U} = 0$.

(b) $\tilde{U} = 1$.

(c) $\tilde{U} = 2$.

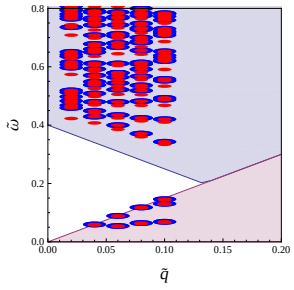

(d) $\tilde{U} = 3$.

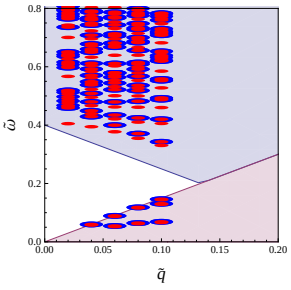

(e) $\tilde{U} = 3.2$.

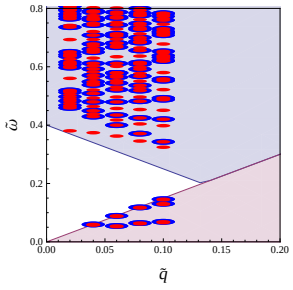

(f) $\tilde{U} = 3.4$.

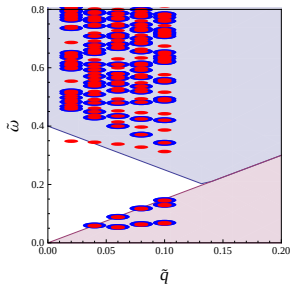

(g) $\tilde{U} = 3.6$.

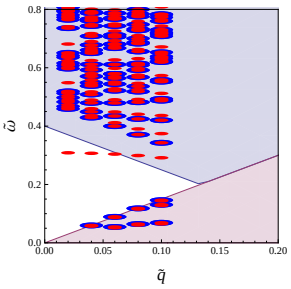

(h) $\tilde{U} = 3.8$.

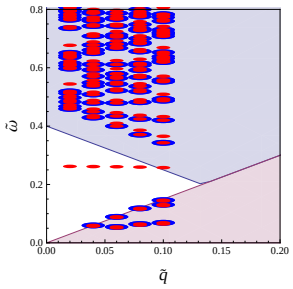

(i) $\tilde{U} = 4.0$.

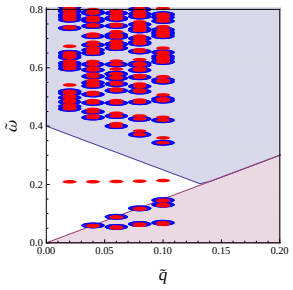

(j) $\tilde{U} = 4.2$.

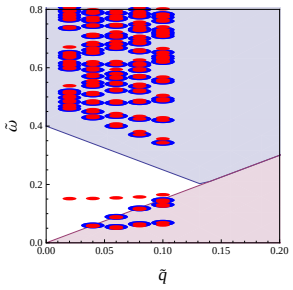

(k) $\tilde{U} = 4.4$.

Figure 4.3: Solutions to the matrix equation Eq. (3.34) for different values of $\tilde{U}$, ranging from 0 to 4.4. The blue disks are eigenvalues of the noninteracting Hamiltonian i.e. when $\tilde{U} = 0$, whereas the red disks are eigenvalues of the full Hamiltonian.

Now we have seen that long living triplet excitations do indeed exist in graphene, which represents a bound state formation. The frequency of the modes $\omega_{\tilde{q}}$ depends on $\tilde{U}$ but they can be quantized giving oscillatory quanta called magnons with a characteristic frequency $\omega_{\tilde{q}}$. We would like to analyze those in more details and for doing that we choose the dispersion relation for $\tilde{U} = 4.0$. In Fig 4.4(a) we show again the whole excitation spectrum for the chosen value of the interaction strength evaluated for five different directions of $\tilde{q}$ of same length in the I quadrant of the coordinate system. On Fig. 4.4(b) we have zoomed into the dispersion relation which looks like it is constant on Fig 4.4(a) but appears to be slightly parabolic with negative curvature.

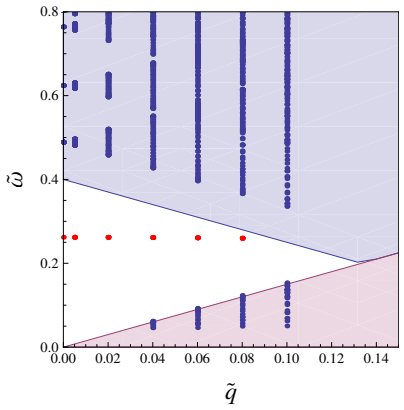

(a) The whole excitation spectrum for $\tilde{U} = 4.0$ evaluated for five different directions for $\tilde{q}$ of same length.

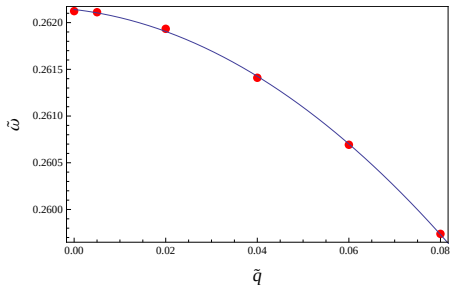

(b) The dispersion relation for $\tilde{U} = 4.0$ having parabolic form. Note the range on the y-axis is very small indicating a small curvature.

Figure 4.4: The excitation spectrum showing both eigenvalues for the noninteracting Hamiltonian and the eigenvalues in the window for the interacting Hamiltonian. To right we show the dispersion relation and a parabolic fit to it.

The fit to the dispersion relation is

$$\tilde{\omega}_{\tilde{q}} = 0.26214 - 0.00561577\tilde{q} - 0.3061137\tilde{q}^2, \tag{4.13}$$

from where we can determine interesting properties of the excitations. First the group velocity, given by the expression

$$\tilde{v}_g = \frac{\mathrm{d}\tilde{\omega}}{\mathrm{d}\tilde{q}} \tag{4.14}$$

$$= -0.00561577 - 0.612273\tilde{q}. \tag{4.15}$$

Multiplying with $\frac{ta_{c-c}}{\hbar}$, having units of velocity gives

$$v_g = -3392\,\mathrm{m/s} - 369850\,\mathrm{m/s}\,\tilde{q}. \tag{4.16}$$

Now we can determine the minimum and maximum velocity of the magnons since $\tilde{q}_{min} = 0$ and $\tilde{q}_{max} \simeq 0.09$ giving

$$v_{g_{min}} = -3392\,\mathrm{m/s}, \tag{4.17}$$
$$v_{g_{max}} = -52706\,\mathrm{m/s}. \tag{4.18}$$

The velocities are negative indicating the magnons are moving in the opposite direction of $\mathbf{q}$. The velocity of the magnons are all within $\sim 5\%$ of the Fermi velocity in graphene. We can also determine the effective mass with the following expression

$$\tilde{m}^* = \left(\frac{\mathrm{d}^2\tilde{\omega}}{\mathrm{d}\tilde{q}^2}\right)^{-1} \tag{4.19}$$
$$= -1.63326. \tag{4.20}$$

To convert this number to something we understand we multiply it with $\frac{\hbar^2}{a_{c-c}^2 t}$, having units of mass, and divide by the electron mass $\mathrm{m_e}$ which gives

$$m^* = -5\,\mathrm{m_e}. \tag{4.21}$$

The magnons are heavy, confirmed by Eq. (4.21) but the fact they exists and can be mobilized in spin transport experiments makes them very interesting. In the next chapter we will see how the magnons appear in real space.

Chapter 5

Magnons in real space

In this last chapter of research we analyze how the magnons appear in real space and calculate their spatial probability distribution.

5.1 Transformation to real space

In Section 3.2 we narrowed our research for interesting excitations from the ground state of graphene, to a subspace of the Hilbert space only consisting of linear combination of triplet electron–hole pairs. The expression for these excited states was given as

$$A^\dagger_{\mathbf{q}}|FS\rangle = \sum_{\mathbf{k}\beta\beta'} a_{\mathbf{k}\beta\beta'} c^\dagger_{\mathbf{k}\beta\uparrow} c_{\mathbf{k}-\mathbf{q}\beta'\downarrow}|FS\rangle, \tag{5.1}$$

where $A^\dagger_{\mathbf{q}}$ is a triplet excitation operator with wave vector $\mathbf{q}$. Now we know that the coefficients $a_{\mathbf{k}\beta\beta'}$ are elements of the eigenvectors of Hamiltonian matrix from Eq. (3.34) where $\mathbf{k}$ is of course the wave vector, β the sign of the energy of the electron and β' the sign of the energy of the hole. What we have also given arguments for is that β must be $+$, giving

$$A^\dagger_{\mathbf{q}}|FS\rangle = \sum_{\mathbf{k}\beta'} a_{\mathbf{k}+\beta'} c^\dagger_{\mathbf{k}+\uparrow} c_{\mathbf{k}-\mathbf{q}\beta'\downarrow}|FS\rangle \tag{5.2}$$

$$= \sum_{\mathbf{k}} a_{\mathbf{k}++}\, c^\dagger_{\mathbf{k}+\uparrow} c_{\mathbf{k}-\mathbf{q}+\downarrow}|FS\rangle + \sum_{\mathbf{k}} a_{\mathbf{k}+-}\, c^\dagger_{\mathbf{k}+\uparrow} c_{\mathbf{k}-\mathbf{q}-\downarrow}|FS\rangle. \tag{5.3}$$

In Eq. (5.3) we see the two type of excitations, intraband and interband. Since we Fourier transformed the interaction term in the Hubbard Hamiltonian we have been investigating its properties in reciprocal space. What we can do now is to go back to real space i.e. Fourier transform back and examine how the excitations we found in Section 4.2 appear there. The Fourier transform of the

operators are

$$c^\dagger_{\mathbf{k}\beta\sigma} = \frac{1}{\sqrt{N}} \sum_{i\alpha} \mathrm{e}^{\mathrm{i}\mathbf{k}\cdot\mathbf{R}_i} U_{\mathbf{k}\alpha\beta} c^\dagger_{i\alpha\sigma}, \tag{5.4a}$$

$$c_{\mathbf{k}\beta\sigma} = \frac{1}{\sqrt{N}} \sum_{i\alpha} \mathrm{e}^{-\mathrm{i}\mathbf{k}\cdot\mathbf{R}_i} U^*_{\mathbf{k}\alpha\beta} c_{i\alpha\sigma}, \tag{5.4b}$$

gotten from Eq. (2.38). The matrix elements we write out explicitly as

$$\underline{\underline{U_\mathbf{k}}} = \begin{pmatrix} U_{\mathbf{k}A+} & U_{\mathbf{k}B+} \\ U_{\mathbf{k}A-} & U_{\mathbf{k}B-} \end{pmatrix} = \frac{1}{\sqrt{2}} \begin{pmatrix} -1 & \mathrm{e}^{-\mathrm{i}\phi_\mathbf{k}} \\ \mathrm{e}^{\mathrm{i}\phi_\mathbf{k}} & 1 \end{pmatrix}, \tag{5.5a}$$

$$\underline{\underline{U^*_\mathbf{k}}} = \begin{pmatrix} U^*_{\mathbf{k}A+} & U^*_{\mathbf{k}B+} \\ U^*_{\mathbf{k}A-} & U^*_{\mathbf{k}B-} \end{pmatrix} = \frac{1}{\sqrt{2}} \begin{pmatrix} -1 & \mathrm{e}^{\mathrm{i}\phi_\mathbf{k}} \\ \mathrm{e}^{-\mathrm{i}\phi_\mathbf{k}} & 1 \end{pmatrix}. \tag{5.5b}$$

Now we have all ingredients to write Eq. (5.3) out in real space and what we get is

$$\begin{aligned} A^\dagger_\mathbf{q}|FS\rangle = \sum_\mathbf{k} a_{\mathbf{k}++} \Bigg(& \frac{1}{\sqrt{N}} \sum_i \mathrm{e}^{\mathrm{i}\mathbf{k}\cdot\mathbf{R}_i} \frac{1}{\sqrt{2}} \left(-c^\dagger_{iA\uparrow} + \mathrm{e}^{-\mathrm{i}\phi_\mathbf{k}} c^\dagger_{iB\uparrow} \right) \\ & \frac{1}{\sqrt{N}} \sum_j \mathrm{e}^{-\mathrm{i}(\mathbf{k}-\mathbf{q})\cdot\mathbf{R}_j} \frac{1}{\sqrt{2}} \left(-c^\dagger_{jA\downarrow} + \mathrm{e}^{\mathrm{i}\phi_{\mathbf{k}-\mathbf{q}}} c^\dagger_{jB\downarrow} \right) \Bigg) |FS\rangle \\ + \sum_\mathbf{k} a_{\mathbf{k}+-} \Bigg(& \frac{1}{\sqrt{N}} \sum_i \mathrm{e}^{\mathrm{i}\mathbf{k}\cdot\mathbf{R}_i} \frac{1}{\sqrt{2}} \left(-c^\dagger_{iA\uparrow} + \mathrm{e}^{-\mathrm{i}\phi_\mathbf{k}} c^\dagger_{iB\uparrow} \right) \\ & \frac{1}{\sqrt{N}} \sum_j \mathrm{e}^{-\mathrm{i}(\mathbf{k}-\mathbf{q})\cdot\mathbf{R}_j} \frac{1}{\sqrt{2}} \left(\mathrm{e}^{-\mathrm{i}\phi_{\mathbf{k}-\mathbf{q}}} c^\dagger_{jA\downarrow} + c^\dagger_{jB\downarrow} \right) \Bigg) |FS\rangle. \end{aligned} \tag{5.6}$$

We can take the sums out of the parentheses and collect the exponential functions to get

$$\begin{aligned} A^\dagger_\mathbf{q}|FS\rangle = & \frac{1}{2N} \sum_\mathbf{k} \sum_{ij} a_{\mathbf{k}++} \, \mathrm{e}^{\mathrm{i}(\mathbf{k}\cdot(\mathbf{R}_i-\mathbf{R}_j)+\mathbf{q}\cdot\mathbf{R}_j)} \left(-c^\dagger_{iA\uparrow} + \mathrm{e}^{-\mathrm{i}\phi_\mathbf{k}} c^\dagger_{iB\uparrow} \right) \\ & \times \left(-c^\dagger_{jA\downarrow} + \mathrm{e}^{\mathrm{i}\phi_{\mathbf{k}-\mathbf{q}}} c^\dagger_{jB\downarrow} \right) |FS\rangle \\ & + \frac{1}{2N} \sum_\mathbf{k} \sum_{ij} a_{\mathbf{k}+-} \, \mathrm{e}^{\mathrm{i}(\mathbf{k}\cdot(\mathbf{R}_i-\mathbf{R}_j)+\mathbf{q}\cdot\mathbf{R}_j)} \left(-c^\dagger_{iA\uparrow} + \mathrm{e}^{-\mathrm{i}\phi_\mathbf{k}} c^\dagger_{iB\uparrow} \right) \\ & \times \left(\mathrm{e}^{-\mathrm{i}\phi_{\mathbf{k}-\mathbf{q}}} c^\dagger_{jA\downarrow} + c^\dagger_{jB\downarrow} \right) |FS\rangle. \end{aligned} \tag{5.7}$$

At last we expand the parentheses containing the operators

$$\begin{aligned} A^\dagger_{\mathbf{q}}|FS\rangle = \frac{1}{2N}\sum_{\mathbf{k}}\sum_{ij} a_{\mathbf{k}++}\,\mathrm{e}^{\mathrm{i}(\mathbf{k}\cdot(\mathbf{R}_i-\mathbf{R}_j)+\mathbf{q}\cdot\mathbf{R}_j)}\Big(c^\dagger_{iA\uparrow}c_{jA\downarrow} - \mathrm{e}^{\mathrm{i}\phi_{\mathbf{k}-\mathbf{q}}}c^\dagger_{iA\uparrow}c_{jB\downarrow} \\ - \mathrm{e}^{-\mathrm{i}\phi_{\mathbf{k}}}\,c^\dagger_{iB\uparrow}c_{jA\downarrow} + \mathrm{e}^{\mathrm{i}(\phi_{\mathbf{k}-\mathbf{q}}-\phi_{\mathbf{k}})}\,c^\dagger_{iB\uparrow}c_{jB\downarrow}\Big)|FS\rangle \\ + \frac{1}{2N}\sum_{\mathbf{k}}\sum_{ij} a_{\mathbf{k}+-}\,\mathrm{e}^{\mathrm{i}(\mathbf{k}\cdot(\mathbf{R}_i-\mathbf{R}_j)+\mathbf{q}\cdot\mathbf{R}_j)}\Big(-\mathrm{e}^{-\mathrm{i}\phi_{\mathbf{k}-\mathbf{q}}}c^\dagger_{iA\uparrow}c_{jA\downarrow} - c^\dagger_{iA\uparrow}c_{jB\downarrow} \\ - \mathrm{e}^{-\mathrm{i}(\phi_{\mathbf{k}}+\phi_{\mathbf{k}+\mathbf{q}})}\,c^\dagger_{iB\uparrow}c_{jA\downarrow} + \mathrm{e}^{-\mathrm{i}\phi_{\mathbf{k}}}\,c^\dagger_{iB\uparrow}c_{jB\downarrow}\Big)|FS\rangle. \end{aligned} \tag{5.8}$$

The coefficients $a_{\mathbf{k}++}$ and $a_{\mathbf{k}+-}$ are elements of the eigenvectors of Eq. (3.34), when we insert the eigenvectors corresponding the eigenvalues in the window we are calculating the properties of the magnons. What we can see from Eq. (5.8) is that each magnon is a linear combination of four terms representing all possible combinations of an electron in unit cell i and hole in unit cell j. They are

i) Electron at site A and hole at site A.

ii) Electron at site A and hole at site B.

iii) Electron at site B and hole at site A.

iv) Electron at site B and hole at site B.

Eq. (5.8) is an general expression for a triplet excitation having wave vector $\mathbf{q}$ in real space. In Fig. 4.4(a) we saw that for $\hat{q} = 0$ there is a solution in the window of the electron–hole excitation spectrum so we would like to analyze the real space spatial distribution of that magnon. Setting $\mathbf{q} = 0$ in Eq. (5.8) results in

$$\begin{aligned} A^\dagger_{\mathbf{0}}|FS\rangle = \frac{1}{2N}\sum_{\mathbf{k}}\sum_{i} a_{\mathbf{k}+-}\,\mathrm{e}^{\mathrm{i}\mathbf{k}\cdot\mathbf{R}_i}\Big(-\mathrm{e}^{-\mathrm{i}\phi_{\mathbf{k}}}\,c^\dagger_{iA\uparrow}c_{jA\downarrow} - c^\dagger_{iA\uparrow}c_{jB\downarrow} \\ - \mathrm{e}^{-\mathrm{i}2\phi_{\mathbf{k}}}\,c^\dagger_{iB\uparrow}c_{jA\downarrow} + \mathrm{e}^{-\mathrm{i}\phi_{\mathbf{k}}}\,c^\dagger_{iB\uparrow}c_{jB\downarrow}\Big)|FS\rangle, \end{aligned} \tag{5.9}$$

where we have defined $\mathbf{R}_i \equiv \mathbf{R}_i - \mathbf{R}_j$, which corresponds to fix the hole in unit cell j and then we can calculate the probability of finding the electron in unit cell i, relative to the hole. This we are allowed to do because of the translational invariance of the system. The probability only depends on the distance between the electron and the hole, not their exact position. Note in Eq. (5.9) there is only one term whereas there are two terms in Eq. (5.8), that is because for the special case $q = 0$ there are no intraband excitations so the former term in Eq. (5.3) is zero. Now we can calculate the spatial probability distribution of this excitation and that we do by projecting onto Eq. (5.9) with the bra version of

the kets we find on the right hand side. Fixing the hole at unit cell $j = 1$ and calculating the probability amplitudes for finding the electron in unit cell i for the cases i) – iv) from above is then

i) Probability amplitude for finding electron at site A and hole at site A:

$$\langle FS|(c^\dagger_{iA\uparrow}c_{1A\downarrow})^\dagger A^\dagger_0|FS\rangle = -\frac{1}{2N}\sum_{\mathbf{k}} a_{\mathbf{k}+-}\,\mathrm{e}^{\mathrm{i}\mathbf{k}\cdot\mathbf{R}_i}\mathrm{e}^{-\mathrm{i}\phi_{\mathbf{k}}} \tag{5.10}$$

$$= -\frac{1}{2N}a_{\mathbf{k}_1+-}\mathrm{e}^{\mathrm{i}\mathbf{k}_1\cdot\mathbf{R}_i}\mathrm{e}^{-\mathrm{i}\phi_{\mathbf{k}_1}} + \cdots + (-)\frac{1}{2N}a_{\mathbf{k}_N+-}\mathrm{e}^{\mathrm{i}\mathbf{k}_N\cdot\mathbf{R}_i}\mathrm{e}^{-\mathrm{i}\phi_{\mathbf{k}_N}}. \tag{5.11}$$

ii) Probability amplitude for finding electron at site A and hole at site B:

$$\langle FS|(c^\dagger_{iA\uparrow}c_{1B\downarrow})^\dagger A^\dagger_0|FS\rangle = -\frac{1}{2N}\sum_{\mathbf{k}} a_{\mathbf{k}+-}\,\mathrm{e}^{\mathrm{i}\mathbf{k}\cdot\mathbf{R}_i}\mathrm{e}^{-\mathrm{i}2\phi_{\mathbf{k}}} \tag{5.12}$$

$$= -\frac{1}{2N}a_{\mathbf{k}_1+-}\mathrm{e}^{\mathrm{i}\mathbf{k}_1\cdot\mathbf{R}_i}\mathrm{e}^{-\mathrm{i}2\phi_{\mathbf{k}_1}} + \cdots + (-)\frac{1}{2N}a_{\mathbf{k}_N+-}\mathrm{e}^{\mathrm{i}\mathbf{k}_N\cdot\mathbf{R}_i}\mathrm{e}^{-\mathrm{i}2\phi_{\mathbf{k}_N}}. \tag{5.13}$$

iii) Probability amplitude for finding electron at site B and hole at site A:

$$\langle FS|(c^\dagger_{iB\uparrow}c_{1A\downarrow})^\dagger A^\dagger_0|FS\rangle = -\frac{1}{2N}\sum_{\mathbf{k}} a_{\mathbf{k}+-}\,\mathrm{e}^{\mathrm{i}\mathbf{k}\cdot\mathbf{R}_i} \tag{5.14}$$

$$= -\frac{1}{2N}a_{\mathbf{k}_1+-}\mathrm{e}^{\mathrm{i}\mathbf{k}_1\cdot\mathbf{R}_i} + \cdots + (-)\frac{1}{2N}a_{\mathbf{k}_N+-}\mathrm{e}^{\mathrm{i}\mathbf{k}_N\cdot\mathbf{R}_i}. \tag{5.15}$$

iv) Probability amplitude for finding electron at site B and hole at site B:

$$\langle FS|(c^\dagger_{iB\uparrow}c_{1B\downarrow})^\dagger A^\dagger_0|FS\rangle = \frac{1}{2N}\sum_{\mathbf{k}} a_{\mathbf{k}+-}\,\mathrm{e}^{\mathrm{i}\mathbf{k}\cdot\mathbf{R}_i}\mathrm{e}^{-\mathrm{i}\phi_{\mathbf{k}}} \tag{5.16}$$

$$= \frac{1}{2N}a_{\mathbf{k}_1+-}\mathrm{e}^{\mathrm{i}\mathbf{k}_1\cdot\mathbf{R}_i}\mathrm{e}^{-\mathrm{i}\phi_{\mathbf{k}_1}} + \cdots + \frac{1}{2N}a_{\mathbf{k}_N+-}\mathrm{e}^{\mathrm{i}\mathbf{k}_N\cdot\mathbf{R}_i}\mathrm{e}^{-\mathrm{i}\phi_{\mathbf{k}_N}}. \tag{5.17}$$

The probability of finding these different configurations is then of course the squared moduli of the appropriated probability amplitudes,

$$P\left(\begin{matrix}\text{Hole at site A in unit cell j and}\\ \text{electron at site A in unit cell i.}\end{matrix}\right) = \left| -\frac{1}{2N}\sum_{\mathbf{k}} a_{\mathbf{k}+-}\, \mathrm{e}^{\mathrm{i}\mathbf{k}\cdot\mathbf{R}_i}\mathrm{e}^{-\mathrm{i}\phi_{\mathbf{k}}} \right|^2, \tag{5.18}$$

$$P\left(\begin{matrix}\text{Hole at site A in unit cell j and}\\ \text{electron at site B in unit cell i.}\end{matrix}\right) = \left| -\frac{1}{2N}\sum_{\mathbf{k}} a_{\mathbf{k}+-}\, \mathrm{e}^{\mathrm{i}\mathbf{k}\cdot\mathbf{R}_i}\mathrm{e}^{-\mathrm{i}2\phi_{\mathbf{k}}} \right|^2, \tag{5.19}$$

$$P\left(\begin{matrix}\text{Hole at site B in unit cell j and}\\ \text{electron at site A in unit cell i.}\end{matrix}\right) = \left| -\frac{1}{2N}\sum_{\mathbf{k}} a_{\mathbf{k}+-}\, \mathrm{e}^{\mathrm{i}\mathbf{k}\cdot\mathbf{R}_i} \right|^2, \tag{5.20}$$

$$P\left(\begin{matrix}\text{Hole at site B in unit cell j and}\\ \text{electron at site B in unit cell i.}\end{matrix}\right) = \left| \frac{1}{2N}\sum_{\mathbf{k}} a_{\mathbf{k}+-}\, \mathrm{e}^{\mathrm{i}\mathbf{k}\cdot\mathbf{R}_i}\mathrm{e}^{-\mathrm{i}\phi_{\mathbf{k}}} \right|^2. \tag{5.21}$$

In Figs. 5.1 and 5.2 we show the probability distributions for placing the hole denoted with ◯ in unit cell $j = 1$ at site A and B repsectively, and finding the electron somewhere in the lattice within $5\,a_{c-c}$. Unit cell $j = 1$ is sketched on the figures and the probability finding the electron at site A is denoted with a blue disks and finding it at site B with a red disk. The area of the disks is proportional to the probability.

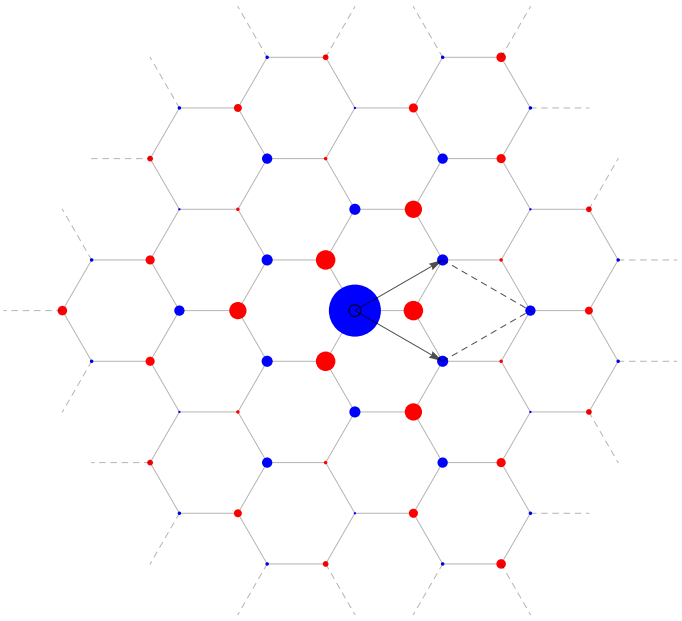

Figure 5.1: The spatial probability distribution for placing the hole in unit cell $j = 1$ at site A and finding the electron somewhere in the lattice within $5\,a_{c-c}$. The area of the disks is proportional to the probability where blue disks are on sublattice A and red disks are on sublattice B.

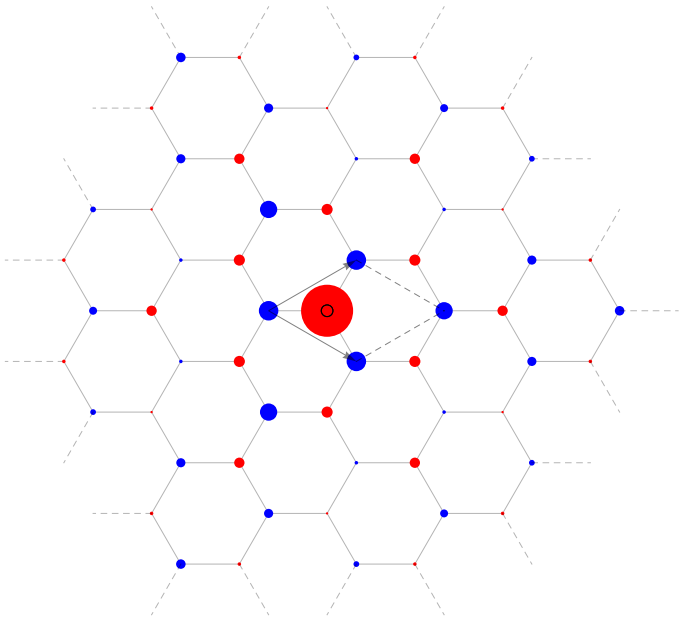

Figure 5.2: The spatial probability distribution for placing the hole in unit cell $j = 1$ at site B and finding the electron somewhere in the lattice within $5\,a_{c-c}$. The area of the disks is proportional to the probability. Blue disks are on sublattice A and red disks are on sublattice B.

As we can see on the figures there is largest probability to find the electron on the same site as the hole which corresponds to a spin-flip i.e. an electron with spin down is annihilated and an electron with spin up is created on the same site. Interestingly in second place it is most likely to find the electron on the other sublattice which is at the hole's nearest neighbors.

In Fig. 5.3 we show the probability of placing the hole at either sublattice A or B and finding the electron at some nearest neighbour within $5a_{c-c}$ where "S" stands for "Same sublattice as hole" and "D" for "Different sublattice than hole". For example, putting the hole at either site A or B then it is $\sim 25\%$ to find the electron at the same site respectively. This is the first spike in Fig. 5.3 having nearest neighbour number 0 since it was the probability of finding the electron at the same site as the hole. The second spike, which shows the probability of finding the electron at the hole's nearest neighbour where the hole is either at site A or B is $\sim 11\%$. This spike is denoted with D since in graphene the nearest neighbour of each carbon atom in graphene is always a part of the opposite sublattice.

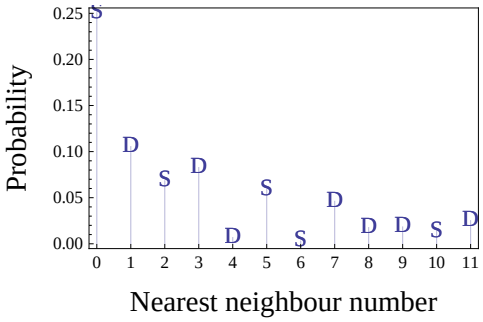

Figure 5.3: The probability distribution for the triplet excitation with $\mathbf{q} = 0$. "S" stands for electron at the same sublattice as hole and "D" for electron at the different sublattice as hole.

Obviously the probability distribution is decreasing as we move away from the position of the hole which indicates a localized excitation in real space. In Fig. 5.4 we show more quantitative results of this behaviour where in (a) we show the probability of finding the electron within given distance from the hole and in (b) we have the virtual graphene crystal under considerations. The black dots on Fig. 5.4(b) denote the unit cells, so there are 1600 of them and the colored circles match the colored dots on Fig. 5.4(a), indicating the distance from the hole. What we can read of these information is of course there is 100% probability of finding the electron within $60a_{c-c}$ from the hole i.e. the electron is somewhere in the crystal. To find the electron within $30a_{c-c}$ from the hole is indicated with blue color and turns out to be $\sim$ 96% probability. Finding the electron within $10a_{c-c}$ is shown with green color and is $\sim$ 82% probability. This strongly implies that the excitation is well localized within few interatomic distances.

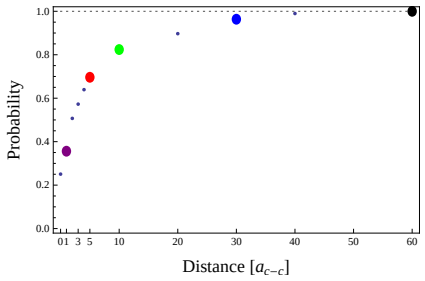

(a) Probability as a function of distance from the hole. For colored dots a circle is drawn in same color in the figure beside.

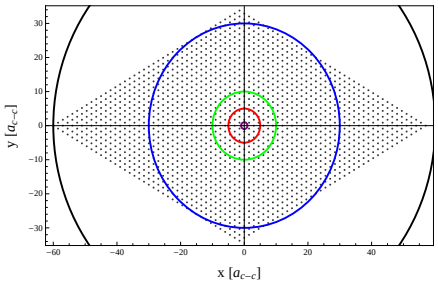

(b) The virtual graphene crystal with 1600 unit cells marked with black dots. The circles indicate determined distances from the hole.

Figure 5.4: Figures showing how the probability of finding the electron decreases as a function of distance from the hole.

What we have considered until now is only the magnon having $\mathbf{q} = 0$, but as we can see on Fig. 4.4(b) they can exists all the up to $\tilde{q} \sim 0.08$ for $\tilde{U} = 4.0$. In Eq. (5.8) we have a general result for any triplet excitation and since we are only interested in the bound states solutions i.e. the undamped magnons we assume the coefficients $a_{\mathbf{k}+\beta'}$ are elements of the appropriated eigenvectors. Like we did for the special case, $\mathbf{q} = 0$, we can define $\mathbf{R}_i \equiv \mathbf{R}_i - \mathbf{R}_j$ which indicates we fix the hole at position $\mathbf{R}_j$ and calculate the position of the electron relative to the hole. Now what the exponent, $\mathbf{q} \cdot \mathbf{R}_j$, in the exponential functions represents is that the center of mass, $\mathbf{R}_j$, has momentum $\mathbf{q}$. The whole excitation will appear exactly the same except its center of mass will have momentum in a certain direction. Drawing a parallel to a hydrogen atom flying across the room, the electron will have the same spatial probability distribution around the proton when in motion and when the atom is stationary.

Chapter 6

Conclusion

To conclude the thesis we briefly state what we have accomplished. We started out by asking questions about the effect of the Coulomb interaction between electrons in graphene. Knowing how the interaction is essential in the world of molecules, it is paradoxical describing a material which can be considered as a giant molecule, by neglecting this interaction. We therefore wanted to include the Coulomb interaction to our description of graphene through the Hubbard Hamiltonian and examine the consequences.

The ground state of graphene consists of the filled Fermi Sea. Excitations from that state can be in different forms. We analyzed specifically triplet excitations from the ground state of doped graphene and found out that the Coulomb interaction drives some of the electron-hole pairs into the window of the electron-hole excitation spectrum. For $U \simeq 11\,\text{eV}$ denoting the strength of the Coulomb interaction a well-defined mode of collective excitations, called magnons, appeared in the window. For that interaction strength the magnons are heavy i.e. have effective mass of $m^* = -5m_e$, but their existence is unambiguous. To gain more insight we Fourier transformed back to real space and analyzed the appearance of magnons there by placing the hole at some arbitrary unit cell in the lattice and calculating the probability of finding the electron. We found out the excitations are well localized where there is largest probability of a spin-flip process but secondly the electron is most likely to reside at the opposite sublattice to the hole. From these results we concluded the magnons are to be found within 10 interatomic distances with 82% probability. The advantage of localization is of great deal when it comes to engineer these excitations in spintronics devices.

But how to detect these magnetic excitations in graphene? At least two possible experimental techniques are worth trying:

i) Magnons have been detected in spin transport experiments [21] where spins are pumped from a ferromagnetic media to a nonmagnetic metal, resulting in spin current. This could also be realized using graphene as

a receiver, attached to the ferromagnetic material. On the other end the magnons are then detected by using an inverse spin Hall effect detector.

ii) Magnons could be detected by inelastic neutron scattering. By definition graphene is only one atomic thick and therefore it has the disadvantage that neutrons have large probability of passing through the sample without being affected. It is though realistic to use bulk graphite and decouple the atomic layers, effectively resulting in a crystal containing many layers of graphene. In that case the magnons could be detected indirectly by calculating the energy change of the incoming and outgoing neutron beam.

Magnons can be used for information processing where spin angular momentum is transferred macroscopic distances, this is a key element in spintronics. In addition using the experimental setup described in i) the magnons can be transferred via the graphene crystal between spintronic devices, into molecules or into molecular electronic devices.

With these words we end this thesis. There is still a lot to learn about the Coulomb interaction in graphene but we hope we have at least managed to cover one of the holes found in the theory. Our research has shown that the interaction between electrons in graphene is a source for a lot of interesting physics. Those should not be neglected in the process of obtaining full understanding of graphene which then can be utilized due to its unique, superior properties.

References

[1] K. S. Novoselov, A. K. Geim, S. V. Morozov, D. Jiang, Y. Zhang, S. V. Dubonos, I. V. Grigorieva, and A. A. Firsov. Electric field effect in atomically thin carbon films. *Science*, 306, 2004.

[2] Catherine E. Housecroft and Edwin C. Constable. *Chemistry*. Pearson Education Limited, 2006.

[3] Stephen Blundell. *Magnetism in Condensed Matter*. Oxford University Press, 2001.

[4] Per Hedegård. On the origin of ferromagnetism in certain organic molecules. 2011.

[5] H. S. Philip Wong and Deji Akinwande. *Carbon Nanotube and Graphene Device Physics*. Cambridge University Press, 2011.

[6] R. Saito, G. Dresselhaus, and M. S. Dresselhaus. *Physical Properties of Carbon Nanotubes*. Imperial College Press, 2001.

[7] A. K. Geim and K. S. Novoselov. The rise of graphene. 6, 2007.

[8] Neil W. Ashcroft and N. David Mermin. *Solid State Physics*. Saunders College, 1976.

[9] Daniel R. Dreyer, Rodney S. Ruoff, and Christopher W. Bielawski. From conception to realization: An historial account of graphene and some perspectives for its future. *Angewandte Chemie International Edition*, 49, 2010.

[10] Andre K. Geim. Nobel lecture: Random walk to graphene. *Rev. Mod. Phys.*, 83, 2011.

[11] K. S. Novoselov. Nobel lecture: Graphene: Materials in the flatland. *Rev. Mod. Phys.*, 83, 2011.

[12] Nobelprize.org. The nobel prize in physics 2010, Juni 2012.

[13] Jari Kinaret, Vladimir Falko, Andrea Ferrari, Ana Helman, Jani Kivioja, Daniel Neumaier, Konstantin Novoselov, Vincenzo Palermo, and Stephan Roche. Publishable flagship proposal report. Technical report, 2012.

[14] Henrik Bruus and Karsten Flensberg. *Many-Body Quantum Theory in Condensed Matter Physics*. Oxford University Press, 2004.

[15] Kei Yosida. *Theory of Magnetism*. Springer, 1991.

[16] Piers Coleman. *Introduction to Many Body Physics*. Cambridge University Press, 2011.

[17] Hal Tasaki. The hubbard model: Introduction and selected rigorous results. *J. Phys.: Condens. Matter*, 10, 1998.

[18] A. H. Castro Neto, F. Guinea, N. M. R. Peres, K. S. Novoselov, and A. K. Geim. The electronic properties of graphene. *Rev. Mod. Phys.*, 81, 2009.

[19] Helmut G. Kiess. *Conjugated conducting polymers*. Springer, 1992.

[20] T. O. Wehling, E. Sasioglu, C. Friedrich, A. I. Lichtenstein, M. I. Katsnelson, and S. Blügel. Strength of effective coulomb interactions in graphene and graphite. *Phys. Rev. Lett.*, 106, 2011.

[21] A. V Chumak, A. A. Serga, M. B. Jungfleisch, R. Neb, D. A. Bozhko, V. S. Tiberkevich, and B. Hillebrands. Direct detection of magnon spin transport by the inverse spin hall effect. *Appl. Phys. Lett.*, 10, 2012.

A The Mathematica code

```
acc = 1; (*carbon-carbon distance set to 1*)
R1 = {acc, 0}; (*nearest neighbour vector to B in same unit cell*)
θ = 2π/3;
RotMat = ( Cos[θ]  -Sin[θ] )
         ( Sin[θ]   Cos[θ] );
R2 = RotMat.R1 (*nearest neighbour vector*)
R3 = RotMat.R2(*nearest neighbour vector*)
a1 = R1 - R3 (*real space lattice vector*)
a2 = R1 - R2(*real space lattice vector*)
A3 = {0, 0, 1}; (*3d real space lattice vector*)
A1 = Append[a1, 0]; (*3d real space lattice vector*)
A2 = Append[a2, 0]; (*3d real space lattice vector*)
B1 = 2π (A2×A3)/((A2×A3).A1); (*3d recriprocal space lattice vector*)
B2 = 2π (A3×A1)/((A3×A1).A2); (*3d recriprocal space lattice vector*)
B3 = 2π (A1×A2)/((A1×A2).A3); (*3d recriprocal space lattice vector*)
b1 = Drop[B1, -1](*reciprocal lattice vector*)
b2 = Drop[B2, -1](*reciprocal lattice vector*)
K1 = {0, 4π/(3√3)}(*Dirac point*)
K2 = {0, -4π/(3√3)}(*Dirac point*)
K = {2π/3, 2π/(3√3)}(*Dirac point*)
mK = {-2π/3, 2π/(3√3)}(*Dirac point*)
K' = {2π/3, -2π/(3√3)}(*Dirac point*)
mK' = {-2π/3, -2π/(3√3)}(*Dirac point*)
f[k_] := 1 + Exp[-i k.a1] + Exp[-i k.a2](*f(k)*)
eps[k_] := Abs[f[k]](*dispersion relation*)
```

Out[111]= $\left\{-\frac{1}{2}, \frac{\sqrt{3}}{2}\right\}$

Out[112]= $\left\{-\frac{1}{2}, -\frac{\sqrt{3}}{2}\right\}$

Out[113]= $\left\{\frac{3}{2}, \frac{\sqrt{3}}{2}\right\}$

Out[114]= $\left\{\frac{3}{2}, -\frac{\sqrt{3}}{2}\right\}$

Out[121]= $\left\{\frac{2\pi}{3}, \frac{2\pi}{\sqrt{3}}\right\}$

Out[122]= $\left\{\frac{2\pi}{3}, -\frac{2\pi}{\sqrt{3}}\right\}$

Out[123]= $\left\{0, \frac{4\pi}{3\sqrt{3}}\right\}$

Out[124]= $\left\{0, -\frac{4\pi}{3\sqrt{3}}\right\}$

Out[125]= $\left\{\frac{2\pi}{3}, \frac{2\pi}{3\sqrt{3}}\right\}$

Out[127]= $\left\{\frac{2\pi}{3}, -\frac{2\pi}{3\sqrt{3}}\right\}$

Out[128]= $\left\{-\frac{2\pi}{3}, -\frac{2\pi}{3\sqrt{3}}\right\}$

```
kmu02 = 0.2 / (3/2);(*k_μ*)

DOS02 = RegionPlot[{ω > 3/2 q && ω > 3/2 (-q + 2 kmu02), ω > 3/2 (q - 2 kmu02) && ω < 3/2 q},
  {q, 0, 1.0}, {ω, 0, 2.0}, PlotRange → {{0, 1.0}, {0, 2.0}}, Frame → True,
  FrameLabel -> {Text[Style["q̃", FontSize → 15]], Text[Style["ω̃", FontSize → 15]]},
  FrameTicks → {{Automatic, None}, {Automatic, None}}, ImageSize → 250];
(*electron-hole excitation spectrum*)

U[k_] := (z = f[k]; az = z / Abs[z]; 1/√2 ( -1  Conjugate[az] ; az  1 ))(*U matrix*)

MakeBasis[q_, μ_, n_, max_] := Module[
  {bas},
  bas = {};
  kTab = Flatten[Table[N[i b1/n + j b2/n], {i, 0, n - 1}, {j, 0, n - 1}], 1];
  Map[
   If[
     max > eps[#] > μ && eps[# - q] < μ , AppendTo[bas, {#, 1}]
     (*positive hole, having k values less than μ*)
    ]
    &, kTab];
  Map[
   If[
     max > eps[#] > μ && eps[# - q] < max, AppendTo[bas, {#, 2}]
     (*negative hole,  eps[#-q] < max -> the hole can have any k value. *)
    ]
    &, kTab];

  bas

 ]
(*function to make the basis of k-
 values according to interband and intraband excitations*)
```

```
MakeHam[UU_, NN_, basis_, q_] := Module[{},
  Umats = Map[U[#[[1]]] &, basis];
  (*List of matrices for all the different k values*)
  Uqmats = Map[U[#[[1]] - q] &, basis];
  Diag = Map[(eps[#[[1]]] - If[#[[2]] == 1, 1, -1] eps[#[[1]] - q]) &, basis];
  (*List of diagonal elements ϵ±ϵ depending on if the hole is under or over.*)
  nbas = Table[i, {i, Length[basis]}];
  h0 = Outer[H0, nbas, nbas];
  hi = Outer[Hint, nbas, nbas];
  h0 - UU/NN hi]
H0[i_, j_] := If[i == j, Diag[[i]], 0]
Hint[i_, j_] :=
 Umats[[i, 1, 1]] Conjugate[ Uqmats[[i, 1, bassi[[i, 2]]]] ]
   Uqmats[[j, 1, bassi[[j, 2]]]] Conjugate[Umats[[j, 1, 1]]] +
  Umats[[i, 2, 1]] Conjugate[Uqmats[[i, 2, bassi[[i, 2]]]]]
   Uqmats[[j, 2, bassi[[j, 2]]]] Conjugate[Umats[[j, 2, 1]]]
(*The first term is the A sublattice and the second term is the B sublattice*)
(*Umats[[a,b,c]],
a is number af matrix in list,
b is row in matrix, if 1 then A sub, if 2 then B sub,
c is element in row.*)
(*c is either 1 or 2, corresponding to positive or negative hole respecively.*)

(*the hamiltonian matrix generated*)
```